JCIM JOURNAL OF CHEMICAL INFORMATION AND MODELING

Pharmaceutical Modeling

SAR-Guided Scoring Function and Mutational Validation Reveal Binding Mode of CGS-8216 at the #1+/#2- Benzodiazepine Site

David C. B. Siebert, Marcus Wieder, Lydia Schlener, Petra Scholze, Stefan Boresch, Thierry Langer, Michael Schnürch, Marko D. Mihovilovic, Lars Richter, Margot Ernst, and Gerhard F. Ecker

J. Chem. Inf. Model., **Just Accepted Manuscript** • DOI: 10.1021/acs.jcim.8b00199 • Publication Date (Web): 20 Jul 2018

ACS Publications

is published by the American Chemical Society. 1155 Sixteenth Street N.W., Washington, DC 20036

SAR-Guided Scoring Function and Mutational Validation Reveal Binding Mode of CGS-8216 at the α1+/γ2− Benzodiazepine Site

David C. B. Siebert[1, ‡], Marcus Wieder[2,3, ‡], Lydia Schlener[2], Petra Scholze[4], Stefan Boresch[3], Thierry Langer[2], Michael Schnürch[1], Marko D. Mihovilovic[1], Lars Richter[2,], Margot Ernst[5], Gerhard F. Ecker[2]*

[1]Institute of Applied Synthetic Chemistry, TU Wien, Getreidemarkt 9/163, 1060 Vienna, Austria

[2]Department of Pharmaceutical Chemistry, University of Vienna, Althanstrasse 14, 1090 Vienna, Austria

[3]Faculty of Chemistry, Department of Computational Biological Chemistry, University of Vienna, Währingerstrasse 17, 1090, Vienna, Austria

[4]Department of Pathobiology of the Nervous System, Center for Brain Research, Medical University of Vienna, Spitalgasse 4, 1090 Vienna, Austria

[5]Department of Molecular Neurosciences, Center for Brain Research, Medical University of Vienna, Spitalgasse 4, 1090 Vienna, Austria

ABSTRACT: The structural resolution of a bound ligand-receptor complex is a key asset to efficiently drive lead optimization in drug design. However, structural resolution of many drug targets still remains a challenging endeavor. In the absence of structural knowledge, scientists resort on structure-activity relationship (SAR) to promote compound development. In this study we incorporated ligand-based knowledge to formulate a docking scoring function which evaluates binding poses for their agreement with known SAR. We showcased this protocol by identifying the binding mode of the pyrazoloquinolinone (PQ) CGS-8216 at the benzodiazepine binding site of the $GABA_A$ receptor. Further evaluation of the final pose by molecular dynamics and free energy simulations revealed a close proximity between PQ's pending phenyl ring and γ2D56 congruent with the low potency of carboxy-phenyl analogues. Ultimately, we introduced the γ2D56A mutation and in fact observed a 10-fold potency increase in the carboxy-phenyl analogue, providing experimental evidence in favour of our binding hypothesis.

INTRODUCTION

The structural resolution of ligand-receptor complexes dramatically accelerates the elaborate multiparameter optimization of a lead structure in drug discovery. The gained insight into binding mode provides a rational basis to drive potency and selectivity improvements[1]. Moreover, medicinal chemists can use the binding orientation of the ligand to optimize ADME parameters, such as solubility and metabolic stability, without disrupting essential ligand-receptor interactions[1,2]. In addition, this information can assist to identify molecular determinants leading, for instance, to agonist and antagonist behavior of ligands [3].

However, structural elucidation of a bound complex itself is a time-consuming endeavor and failed for many important drug targets[4]. In the absence of protein structure information scientists can use different methods to investigate lead compounds. Two prominent approaches are (1) homology modeling and structure-based design[5], as well as (2) structure-activity relationships[6] (SAR) derived from biological evaluation of compound libraries.

Among other factors, the success of homology modeling and subsequent structure-based design depends on the sequence similarity between target and template proteins and the resolution of the template structure[7]. With decreasing structural certainty of the target protein, the chance to correctly identify the correct binding mode declines[8]. In general, docking algorithms have been shown to be able to explore the conformational space sufficiently well to generate the correct binding orientation, however scoring functions often fail to correctly rank them[9] . In this context the proper algorithmic representation of complex processes like entropy, solvation and protein flexibility remains a big challenge in pose scoring[10,11]. However, more elaborate methods like molecular dynamics (MD) simulations and free energy simulations (FES) describe these processes more accurately and should perform better in such specific cases[12,13]. Nevertheless, over the last years the Drug Design Data Resource (D3R) challenges[14] for protein-ligand pose and affinity predictions have shown impressively that there is no one method 'to rule them all'. In the latest D3R Grand Challenge the two best performing methods for pose prediction were molecular docking and MD simulations (according to the D3R Grand

Challenge 2)[15]. Thus, a combined methodology implementing the best of both worlds might be a promising approach.

In the absence of a reliable structural model, scientists focused on the identification of structure-activity relationships derived from biological profiling of scaffold analogues to drive lead optimization[6]. In this context the $GABA_A$ receptors represent prominent examples of clinically important targets for drugs like benzodiazepines (BZ), barbiturates, neuroactive steroids, anesthetics and anticonvulsants[16]. In mammals, $GABA_A$ receptors are a heterogeneous group of pentameric receptors assembled from a pool of nineteen possible subunits. In the central nervous system the majority of receptors is composed of two α, two β and one γ subunits (Figure 1A)[17]. BZs exert their anxiolytic, muscle-relaxant, sedative-hypnotic and anticonvulsant effects by binding to an allosteric site located at the extracellular α+/γ– subunit interface (Figure 1B, C)[18]. Generally, a high number of different chemotypes was developed that targets various high affinity BZ-binding sites in the search for selective agents to be used, e.g. for anxiolysis[19]. Exhaustive SAR-analyses were performed for several compound classes which led to an high amount of pharmacological activity data[20–23].

Among the promising chemotypes, the PQs displayed high potential as non-sedative anxiolytics and as benzodiazepine antagonists respectively[23]. From this development two valuable tool compounds, CGS-8216 (Figure 1D) and its chloro-derivative CGS-9896, emerged for *in vitro* and *ex vivo* work[24]. Pharmacokinetic issues and inconclusive *in vivo* profiling of partial agonism and antagonism across different $GABA_A$ receptor subtypes precluded further developments of these compounds into clinics[25]. Recent work indicated that modulatory effects of many PQs in most αβγ receptors are predominantly exerted *via* an alternative allosteric binding site at the "homologues" α+/β– interface[26] while effects at the high affinity BZ-sites in most subtypes are "antagonistic", i.e. flumazenil-like[27,28]. Thus, revisiting the PQs as valuable class of benzodiazepine antagonists due to their sub-nanomolar affinity towards the α+/γ– interfaces appears to be promising.

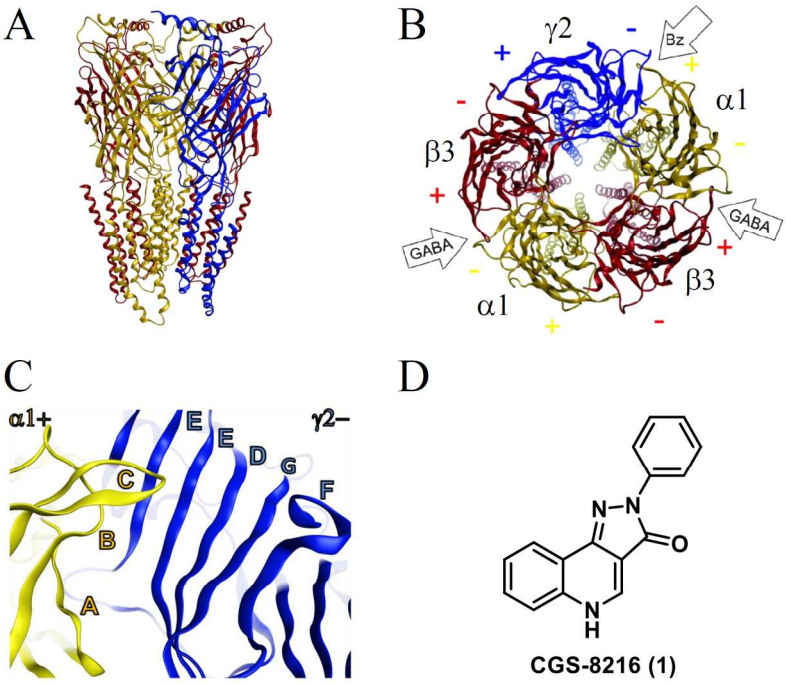

Figure 1: (A) Side view and (B) top view of an α1β3γ2 $GABA_A$ receptor homology model based on the human β3 homopentameric crystal structure 4COF without the intracellular domain. The agonist binding sites (GABA) at the β3+/α1− interfaces and the benzodiazepine binding site (BZ site) at the α1+/γ2− interface are indicated by arrows. α subunits are depicted in yellow, β subunits in red and the γ subunit in blue. (C) α1+/γ2− extracellular interface shaped by loops A-C of the α+ side and loops D-G of the γ2− side. (D) 2D representation of CGS-8216.

CGS-8216 (2-phenyl-2H-pyrazolo[4,3-c]quinolin-3(5H)-one) has been widely used as an essential tool compound for the benzodiazepine binding site. In the past 30 years, scientists have synthesized and tested PQ analogues as BZ-site ligands leading to a highly differentiated SAR of this scaffold[23,29]. Interestingly, the PQs show both, characteristics of 'continuous' as well as 'discontinuous' SAR[30], depending on the respective scaffold substitution sites. Continuous SAR is characterized by a flat activity hypersuperface - here even large structural changes on a molecular scaffold only slightly influence the biological response. Discontinuous SAR, in contrast, is described by a hilly activity hypersuperface, small structural changes can lead to drastic changes in potency.

The described scenario, low-reliability in protein structural information on the one hand and SAR knowledge on the other hand is common for many scaffolds binding to membrane-bound drug targets. While the combination of ligand-based approaches, such as, 3D-shape-matching, pharmacophore mapping and 2D-QSAR with structure-based approaches are widely applied in virtual screening[31–33], they are less common to assist binding mode prediction. Varela et al[34] utilized 3D-similarity and machine learning to augment binding mode prediction. In another study[35], the authors coupled electronic reactivity calculation, multiple-instance learning and molecular docking to predict CYP-mediated sites of metabolism. However, most ligand-, structure-based combinations that rely on SAR data from a congeneric series, analyze only a small number of poses, mostly a single, best-score pose[36–38]. Hence, a potential pose with high SAR congruence but a slightly higher energetic scoring value might be missed by such a procedure.

Given the current challenges of molecular docking into homology models[10] and the simultaneous availability of a highly differentiated SAR for PQ[23], we developed in this study a protocol which integrates the ligand based knowledge in the process of docking pose evaluation. For this purpose, we formulated a SAR scoring function which enabled the systematic assessment of a large CGS-8216 docking pose library for their SAR congruency. The favorite binding hypothesis, characterized by a high SAR_{Score}, was reconfirmed by sophisticated MD analysis composed of relative free energy calculations[39] and stability analysis. Ultimately, we provide experimental evidence for our binding hypothesis by synthesis and testing of PQ analogues in radioligand displacement assays. In line with our computationally derived binding hypothesis, the PQ-analogue carrying a carboxy-phenyl moiety showed a 10-fold potency increase in the $\alpha1\beta3\gamma2$-D56A mutant compared to the $\alpha1\beta3\gamma2$ receptor wild type.

METHODS

Homology model of the α1β3γ2 $GABA_A$ receptor. In order to determine the binding mode of PQs at the extracellular α1+/γ2− interface (benzodiazepine binding site) a homology model based on 4COF[40] was created consisting of two α1, two β3 and one γ2 subunits using Modeller[41] as described previously[42]. The transmembrane domains of the heteropentamer were truncated to obtain a model consisting of the extracellular domains only in order to accelerate MD simulations.

Molecular Docking with GOLD. Molecular docking was performed using *GOLD v1.6.2*[43]. The putative binding site was defined by a cut-off distance of 11.5 Å around the residue S204 of the C-loop of the α1 subunit. Further, we selected ten amino acids with flexible side chains (γ2Y58, γ2F77, γ2T142, α1H101, α1Y159, α1V202, α1S204, α1S205, α1T206 and α1Y209) and set a soft potential to increase to backbone flexibility of the C-loop (α1S204, α1S205, α1T206 and α1G207). The ligand CGS-8216 was minimized using the MMFF94 force field[44] within MOE2016.08[45] prior to docking. To ensure convergence of the sampling, 100 genetic algorithm runs were performed and the GoldScore[46] scoring function was used to retain the 100 best scored poses. Finally, each ligand-receptor complex of the final pose pool was minimized using the LigX energy minimize tool within MOE to relieve potential clashes caused by the soft potential protocol in the docking procedure.

Post-docking derivatization and SAR scoring. The post-docking derivatization was conducted by a customized SVL script using the MOE-SVL built-in function *sm_Build*. This function enables the addition and deletion of atoms on a molecular scaffold. On the basis of the 3D coordinates of each CGS-8216 docking pose (p_1 - p_{100}), an array of eight (**2-9**) analogue placements with *sm_Build* was created. This step expanded the dataset from initial 100 CGS-8216 docking poses to 800 additional post-docking derived analogue placements.

Steric clash energies ($clash_{bb}$ and $clash_{sc}$) were calculated for the derivatized placements p_i*>>cpd 2-4* and p_i*>>cpd 6-9* using the MOE built in SVL function *pro_CheckVDWContacts*. The function returns

clash scores defined as repulsion interaction energy (kcal/mol) for the respective analogue placement. The H-bond interaction strength (h_{bond}) between the N5 nitrogen in CGS-8216 docking poses and the binding site were calculated using the SVL built-in function *prolig_Calculate*.

Interatomic distance (d) calculation. The distances between atoms of the carboxylate moiety of *p_i>>cpd 5 placements* and the carboxylate group atoms of the closest aspartate or glutamate residue were calculated using the SVL built-in function *aDist*. From these distances the shortest interatomic distance between the carboxylate group of the ligand and the receptor was kept.

The SAR scoring function is composed of four subfunctions*: InAct.clash, N5.eval*, *pcarboxy.dist* and *Act.clash*. Each of these take the post-docking engineered analogue geometries, *p_i>>cpd 2-9* as its input (Figure S1) to evaluate the SAR agreement of a docking pose. To assess the SAR of steric hindrance (R^6, R^{6-7}), the *InAct.clash* evaluates clash energies of *p_i>>cpd 2-3* placements (Figure S1B). As the protocol does not include a minimization step after the post-docking derivatization, clashes with rigid structures such as backbone and C_β atoms ($clash_{bb}$) and sidechain atoms ($clash_{sc}$) were weighted distinctly. The *N5.eval* function evaluates both, potential steric hindrance or a disrupted hydrogen bond interaction with quinoline nitrogen (Figure S1C). The PQ-SAR suggests a strong electrostatic repulsion between the 4'-carboxylate moiety and the pocket environment. The *pcarboxy.eval* function evaluates if the 4'-carboxylate moiety of *p_i>>cpd 5* is placed in the vicinity (< 4 Å) of an aspartate or glutamate carboxylate moiety (Figure S1D) by simple distance calculation. The steric tolerance at R^{7-8}, R^8, R^{8-9} and $R^{4'}$ (Figure 2) was assessed via the *Act.clash* subfunction, utilizing the clash energies of *p_i>>cpd 6-9* placements (Figure S1E).

Multidimensional Scaling (MDS) of the pose space. The SVL-exchange script MOL_RMSD.SVL[47] was used to compute the RMSD matrix of the 100 CGS-8216 docking poses. The matrix served as input for MDS to visualize the geometric similarity between poses. The MDS was conducted within the R environment[48] utilizing the *mds* function of the *smacof* R package[49]. The first two dimensions were used to visualize the pose space.

Molecular dynamics simulations and postprocessing. The CHARMM-GUI web interface[50] was used to solvate the homology model of the intracellular GABA-ligand complex and to set up the simulations. All MD simulations were carried out with CHARMM[51], utilizing the CHARMM/openMM coupling[52,53]. Parameters and molecular topologies for the ligands were generated based on the CGenFF force field[54] obtained from *ParamChem* (https://cgenff.paramchem.org/). The protein-ligand complexes were solvated in cubic boxes of TIP3P water[55]. Ions were added to compensate the net charge of the protein-ligand complex and to set the ion concentration to 0.15 M KCI. Electrostatic interactions were computed using the particle-mesh-Ewald method[56]. SHAKE was used to keep all bonds involving hydrogen atoms rigid.

After initial equilibration for 500 ps with a 1 fs time step, each system was simulated for 50 ns using Langevin dynamics at 303.15 K; the pressure was kept around 1 atm by a Monte Carlo barostat. The time step of the production calculation was 2 fs; coordinates were saved every 10 ps, resulting in 5,000 coordinate sets per simulation. For every system ten MD simulations started from the same initial coordinates but with different, randomly seeded velocities were performed. The stability of the simulations was monitored by computing root mean square deviations for the protein and ligand, using the MDAnalysis package[57], as well as visual inspection of the trajectories. The RMSDs were calculated as follows: all coordinates saved during the MD were fitted against the starting structure based on the coordinates of the C_α-atoms of the protein. Using the starting structure as reference, we computed for these reoriented coordinates the RMSD of the C_α-atoms for the protein and the RMSD of the heavy atoms of the ligand. For further calculation the average of the RMSD values of the ligand for the different coordinate sets of a simulation is used (subsequently called L-RMSD in accordance with Liu *et al.*[58]). The protein and ligand RMSD plots of the simulations (RMSD vs simulation time) are available in the SI section. Two tests were performed using the L-RMSD: first, the average of the L-RMSD values of the 10 independent simulations was calculated, i.e. one L-RMSD value was generated that represents the 10 simulations and indicates the stability of the ligand for the binding ode. This value is indicated in the manuscript by using angular brackets and typed as <L-RMSD>. Furthermore, the

number of MD simulations that have a L-RMSD value below a threshold value (in this manuscript we used 2.0 □ in accordance with Liu *et al.*[58]) were also evaluated. This test is a further indicator for the stability of the ligand in the binding pocket - if the L-RMSD value of the majority of the simulations is below the threshold a single simulation with a high L-RMSD value can be set in context.

Additionally, the types of protein-ligand interactions (ionic interactions, hydrophobic interactions, aromatic and hydrogen bond interactions) were analysed for the MD simulations of the different poses using an interaction matrix. This matrix was generated by obtaining a structure-based pharmacophore model for every saved coordinate set of the MD simulation for a specific binding site and subsequently analysing the frequency of the individual features. The pharmacophore feature definitions are in accordance with the definitions used by LigandScout[59].

The maximum possible frequency value corresponds to the length of the simulation, i.e., for 50 ns the maximum number a specific feature can appear is 5,000. Since the ten MD simulations for each pose were accumulated in a single interaction map, the maximum number an interaction could be formed was 50,000. The columns of the interaction matrix indicate all amino acid residues that are involved in an interaction at some point during the MD simulation, the rows designate different parts of the ligand and the color in the matrix indicate how often a specific amino acid was involved in a specific pharmacophore feature. In this way it is possible to analyze the number of interaction partners and also their frequency.

The naming for the columns was in accordance with the following conventions: the letter before the colon indicate the type of interaction. H for hydrophobic, HBA and HBD for hydrogen bond acceptor/donor, PI for positive ionizable interaction and AR for aromatic interaction. This was followed by the one letter residue code and by the residue number of the amino acid. The naming for the rows are in accordance to the labels using in Figure 1. Interactions that appear in fewer than 300 coordinate sets (out of 50,000) were discarded. The interaction map was generated using the python package matplotlib[60] and the chemoinformatic toolkit CDPkit (https://github.com/aglanger/cdpkit).

Free Energy Calculations. Relative free energy differences[61,62] between **5** and **10** were computed employing the usual thermodynamic cycle[63] shown in Figure S2; i.e., we computed the alchemical free energy difference between **5** and **10** in the binding pocket and in solution, respectively. The calculations were carried out for each of the two binding modes considered. To compute the free energy differences of interest, the use of intermediate states in addition to the physical end states of **5** and **10** was required (Figure S3). The technical details and simulation protocols as well as individual results (Table S1) are summarized in the SI section.

Benchmark molecular docking protocols. In total, six different docking protocols were utilized to dock CGS-8216 into the α1β3γ2 $GABA_A$ homology model. From each protocol the best scored pose was kept for comparison studies. The best performing GoldScore[46] and ChemScore[46] poses were filtered from the initial GOLD docking run. In MOE2016.08 the structure preparation protocol was utilized to initialize the system. Then the InducedFit protocol within MOEdock was used to dock CGS-8216 using the default parameters. The best scored poses according to the London dG[64] and the GBVI/WSA dG[65] scoring function were kept. Within the Schrödinger Suite 2015.03 the Protein Preparation Wizard was used to prepare the protein for Schrödinger's Induced Fit docking protocol[66] utilizing default parameters including the Glide SP scoring function.

Molecular docking was also performed using Autodock Vina[67] .For the molecular docking run standard parameters were used, protein flexibility was regarded using flexible side chains (γ2Y58, γ2F77, γ2T142, α1H101, α1Y159, α1V202, α1S204, α1S205, α1T206 and α1Y209) and the exhaustiveness level was set to 16.

$GABA_A$ receptor subunits and mutated subunits. cDNA's of rat $GABA_A$ receptor subunits α1, β3 and γ2S were cloned as described[68]. Mutant γ2S-D56A was constructed using the Q5 Site-Directed Mutagenesis Kit (New England Biolabs) following manufacturer's instruction. We used the wild-type rat γ2-pCI vector as template and the primers ATTCATACAGcTATGTACGTGAAC and

TAATGTTGGTTTCACTCC resulting in a substitution of amino acid D56 (GAT) to A (GCT). The mutated subunit was confirmed by sequencing.

Culturing of human embryonic kidney 293 cells. Human embryonic kidney (HEK) 293 cells (American Type Culture Collection ATCC® CRL-1574™) were maintained in Dulbecco's modified Eagle medium (DMEM, high glucose, GlutaMAX™ supplement, Gibco 61965-059, ThermoFisher, Waltham, Massachusetts, USA) supplemented with 10 % fetal calf serum (Sigma-Aldrich F7524, St. Louis, Missouria, USA), 100 U/ml Penicillin-Streptomycin (Gibco 15140-122, ThermoFisher, Waltham, Massachusetts, USA) and MEM (Non-Essential Amino Acids Gibco 11140-035, ThermoFisher, Waltham, Massachusetts, USA) on 10cm Cell culture dishes (Cell$^+$, Sarstedt, Nürnbrecht, Germany) at 37 °C and 5 % CO_2. HEK293 cells were transfected with cDNAs encoding rat $GABA_A$-receptor subunits subcloned into pCI expression vectors. The ratio of plasmids used for transfection with the calcium phosphate precipitation method [69] were 3 µg α1 : 3 µg β3 and 15 µg γ2 per 10 cm dish. Medium was changed 4-6 hours after transfection. Cells were harvested 72 days after transfection by scraping into phosphate buffered saline. After centrifugation (10 min, 3 000 g, 4 °C) cells were resuspended in TC50 (50 mM Tris-Citrate pH=7.1), homogenized with an ULTRA-TURRAX® (IKA, Staufen, Germany) and centrifuged (10 min, 3 000 g). Membranes were frozen at -20 °C until use.

Radioligand binding assay. [^{3}H]Flunitrazepam (specific activity 83 Ci/mmmol) was purchased from Perkin Elmer NEN (New England Nuclear) (Waltham, Massachusetts, USA). Diazepam (7-chloro-1,3-dihydro-1-methyl-5-phenyl-2H-1,4, benzodiazepine-2-one) from Nycomed (Opfikon, Switzerland). Standard chemicals came from Sigma-Aldrich (St. Louis, Missouri, USA). Frozen membranes were thawed, resuspended in TC50 and incubated for 90 min at 4 °C in a total of 500 µL of a solution containing 50 mM Tris/citrate buffer, pH=7.1, 150 mM NaCl and 2 nM [^{3}H]Flunitrazepam in the absence of presence of either 5 µM diazepam (to determine unspecific binding) or various concentrations of receptor ligands (dissolved in DMSO, final DMSO-concentration 0.5 %). Membranes were filtered through Whatman GF/B filters and the filters were rinsed twice with 4 mL of ice-cold 50

mM Tris/citrate buffer. Filters were transferred to scintillation vials and subjected to scintillation counting after the addition of 3 mL Ultima gold liquid scintillation cocktail. Nonspecific binding determined in the presence of 5 µM Diazepam was subtracted from total [^{3}H]Flunitrazepam binding to result in specific binding. In order to determine the equilibrium binding constant K_D of [^{3}H]Flunitrazepam for the various receptor-subtypes, membranes were incubated with various concentrations of [^{3}H]Flunitrazepam in the absence or presence of 5 µM Diazepam. Saturation binding experiments were analyzed using the equation Y=Bmax*X/(KD+X). Nonlinear regression analysis of the displacement curves used the equation: log(inhibitor) vs. response - variable slope with Top=100 % and Bottom=0 % Y=100/(1+10^((logIC_{50}-x)*Hillslope)). Both analyses were performed using GraphPad Prism version 5.0a for Mac OS X, GraphPad Software, La Jolla California USA, www. graphpad.com. Drug concentrations resulting in half maximal inhibition of specific [^{3}H]Flunitrazepam binding (IC_{50}) were converted to Ki values by using the Cheng-Prusoff relationship [69,70] K_i= IC_{50}/(1+(S/KD)) with S being the concentration of the radioligand (2 nM) (KD values (MW ± SEM, n = 3-4): α1β3γ2S-WT = 7.2 ± 0.2 nM, α1β3γ2S-D56A = 10.3 ± 1.7 nM).

Synthesis. Commercially available reagents were used without further purification. Reactions were monitored by thin layer chromatography with silica gel 60 F_{254} plates (E. Merck, Darmstadt, Germany). ^{1}H and ^{13}C NMR spectra were recorded on Bruker *Avance Ultrashield 400* (^{1}H: 400 MHz, ^{13}C: 101 MHz) or Bruker *Avance IIIHD 600* spectrometer equipped with a Prodigy BBO cryo probe (^{1}H: 600 MHz, ^{13}C: 151MHz). Chemical shifts are reported in parts per million (ppm) and were calibrated using DMSO-d_6 as internal standard. Multiplicities are denoted by s (singlet), br d (broad doublet), d (doublet), dd (doublet of doublet) and m (multiplet). Melting points were determined with a Büchi Melting Point B-545 apparatus. HR-MS was measured on an Agilent 6230 LC TOFMS mass spectrometer equipped with an Aglient Dual AJS ESI-Source. The chromatographic purities of the tested compounds were determined by HPLC analyses on a Nexera system from Shimadzu equipped with 2 binary LC-30AD pumps plus degassers, a CTO-20 column oven and a SPD-M30A PDA detector. Analytical separation was made using a KINETEX C18 column with 1.7 µm pore size and 2.1

x 50 mm length. As solvents HPLC grade water and acetonitrile plus 0.1% formic acid were used (method: gradient of 5% à 95% acetonitrile in water, 12 min, 40°C, 0.5 mL flow, injection volume 3 µL). The purity of all final compounds was >95% (see SI for HPLC analysis).

Diethyl 2-(((4-methoxyphenyl)amino)methylene)malonate. 4-Methoxyaniline (5 g, 36.9 mmol, 1 eq.) and diethyl(ethoxymethylene)malonate (7.46 mL, 36.9 mmol, 1 eq.) were dissolved in toluene (50 mL) and the reaction mixture was heated to reflux. After 22 h the solvent was removed under reduced pressure and the residue was purified by column chromatography (gradient of 10%-30% EtOAc in LP) to give the desired product as yellow crystals (7.90 g, 26.9 mmol, 73%). ^{1}H NMR (400 MHz, $CDCl_3$) δ 1.31 (t, *J* = 7.1 Hz, 3H), 1.37 (t, *J* = 7.1 Hz, 3H), 3.80 (s, 3H), 4.23 (q, *J* = 7.1 Hz, 2H), 4.29 (q, *J* = 7.1 Hz, 2H), 6.86 – 6.94 (m, 2H), 7.05 – 7.10 (m, 2H), 8.43 (d, *J* = 13.9 Hz, 1H), 10.98 (br d, *J* = 13.8 Hz, 1H). ^{13}C NMR (101 MHz, $CDCl_3$) δ 14.5, 14.6, 55.7, 60.1, 60.4, 92.6, 115.1, 119.0, 132.9, 152.8, 157.3, 166.0, 169.4. TLC (PE/EtOAc = 3/1): R_f = 0.63. Mp: 32-34 °C.

Ethyl 6-methoxy-4-oxo-1,4-dihydroquinoline-3-carboxylate. Diethyl 2-(((4-methoxyphenyl)amino)methylene)malonate (2.5 g, 8.52 mmol) was dispersed in diphenylether (15 mL), flushed with argon for 5 min and heated to 235 °C for 1 h. The reaction mixture was poured into LP, the formed precipitate was collected by filtration and washed with LP/EtOAc (1/1, 3 x 40 mL) to yield the desired product as brown powder (1.14 g, 4.62 mmol, 54%). ^{1}H NMR (600 MHz, DMSO-d_6) δ 1.27 (t, *J* = 7.1 Hz, 3H), 3.84 (s, 3H), 4.20 (q, *J* = 7.1 Hz, 2H), 7.34 (dd, *J* = 8.9, 3.0 Hz, 1H), 7.56 (d, *J* = 3.0 Hz, 1H), 7.58 (d, *J* = 9.0 Hz, 1H), 8.49 (d, *J* = 6.7 Hz, 1H), 12.30 (br d, *J* = 6.7 Hz, 1H). ^{13}C NMR (151 MHz, DMSO-d_6) δ 14.4, 55.5, 59.5, 105.5, 108.7, 120.6, 122.2, 128.5, 133.4, 143.7, 156.6, 165.0, 172.9. TLC (2% MeOH in CH_2Cl_2): R_f = 0.33. Mp: 265-267 °C.

Ethyl 4-chloro-6-methoxyquinoline-3-carboxylate. Ethyl 6-methoxy-4-oxo-1,4-dihydroquinoline-3-carboxylate (400 mg, 1.62 mmol) was dispersed in $POCl_3$ (3 mL) and heated to reflux. After 2 h the reaction mixture was poured onto ice, neutralized with satd. $NaHCO_3$, extracted with CH_2Cl_2 (3 x 20 mL), washed with brine (1 x 20 mL), dried over Na_2SO_4, filtered and evaporated. The residue was purified by FC (gradient of 5%-15% EtOAc in LP to give the desired product as colorless crystals (284

mg, 1.08 mmol, 66%). ^{1}H NMR (400 MHz, $CDCl_3$) δ 1.30 – 1.56 (m, 3H), 3.92 (s, 3H), 4.43 (q, *J* = 7.1 Hz, 2H), 7.40 (dd, *J* = 9.2, 2.5 Hz, 1H), 7.53 (d, *J* = 2.5 Hz, 1H), 7.96 (d, *J* = 9.2 Hz, 1H), 8.98 (s, 1H). ^{13}C NMR (101 MHz, $CDCl_3$) δ 14.4, 55.9, 62.2, 103.1, 123.7, 125.1, 127.6, 131.7, 141.4, 145.9, 147.6, 159.5, 164.9. TLC (2% MeOH in CH_2Cl_2): R_f = 0.84. Mp: 88-90 °C.

4-(8-Methoxy-3-oxo-3,5-dihydro-2H-pyrazolo[4,3-c]quinolin-2-yl)benzonitrile. 4-(8-Methoxy-3-oxo-3,5-dihydro-2H-pyrazolo[4,3-c]quinolin-2-yl)benzonitrile was synthesized according to literature [23,27,71] in 57% yield (yellow solid, 202 mg, 0.64 mmol). ^{1}H NMR (400 MHz, DMSO-d_6) δ 3.93 (s, 3H), 7.33 (dd, *J* = 9.1, 2.9 Hz, 1H), 7.60 (d, *J* = 2.9 Hz, 1H), 7.69 (d, *J* = 9.1 Hz, 1H), 7.87 – 7.95 (m, 2H), 8.45 – 8.52 (m, 2H), 8.73 (d, *J* = 6.4 Hz, 1H), 12.97 (br d, *J* = 6.2 Hz, 1H. ^{13}C NMR (101 MHz, DMSO-d_6) δ 55.7, 102.7, 104.6, 105.3, 118.1 (2C), 119.2, 119.8, 120.2, 121.4, 130.0, 133.2 (2C), 138.6, 143.5, 144.3, 157.7, 162.5. HR-MS: calculated [$C_{18}H_{13}N_4O_2^+$]: 317.1033; found [$C_{18}H_{13}N_4O_2^+$]: 317.1038 (diff.: −1.55 ppm). TLC (10% MeOH in CH_2Cl_2): R_f = 0.50. M.p.: decomposes > 300 °C.

4-(8-Methoxy-3-oxo-3,5-dihydro-2H-pyrazolo[4,3-c]quinolin-2-yl)benzoic acid. 4-(8-Methoxy-3-oxo-3,5-dihydro-2H-pyrazolo[4,3-c]quinolin-2-yl)benzonitrile (40 mg, 0.13 mmol) and NaOH (35 mg, 0.89 mmol) were dissolved in 3 mL EtOH/H_2O (v/v) and the reaction mixture was heated to reflux. After 18 h the mixture was acidified wit 2 M HCl and the precipitate was collected by filtration, washed with water (3 mL), LP (15 mL), EtOAc (20 mL) and dried under reduced pressure to give 4-(8-methoxy-3-oxo-3,5-dihydro-2H-pyrazolo[4,3-c]quinolin-2-yl) benzoic acid as yellow solid (28 mg, 0.084 mmol, 66%). ^{1}H NMR (400 MHz, DMSO-d_6) δ 3.95 (s, 3H), 7.33 (dd, *J* = 9.1, 2.9 Hz, 1H), 7.62 (d, *J* = 2.9 Hz, 1H), 7.70 (d, *J* = 9.1 Hz, 1H), 8.04 (d, *J* = 8.5 Hz, 2H), 8.42 (d, *J* = 8.5 Hz, 2H), 8.73 (d, *J* = 6.6 Hz, 1H), 12.79 (br s, 1H), 12.92 (br d, *J* = 6.6 Hz, 1H). ^{13}C NMR (151 MHz, DMSO-d_6) δ 55.7, 102.7, 104.9, 117.6 (2C), 119.9, 120.0, 121.4, 125.5, 129.9, 130.3 (2C), 138.3, 143.6, 143.9, 157.7, 162.3, 167.0. HR-MS: calculated [$C_{18}H_{14}N_3O_4^+$]: 336.0979; found [$C_{18}H_{14}N_3O_4^+$]: 336.0984 (diff.: −1.46 ppm). TLC (20% MeOH in CH_2Cl_2): R_f = 0.57. M.p.: decomposes > 300 °C. HPLC: t_R = 4.64 min (>99.9% purity).

2-(4-Aminophenyl)-8-methoxy-2,5-dihydro-3H-pyrazolo[4,3-c]quinolin-3-one. 2-(4-Aminophenyl)-8-methoxy-2,5-dihydro-3H-pyrazolo[4,3-c]quinolin-3-one was synthesized according to literature[72] in 17% yield (yellow solid, 16 mg, 0.052 mmol). ^{1}H NMR (600 MHz, DMSO-d_6) δ 3.90 (s, 3H), 4.99 (br s, 2H), 6.58–6.64 (m, 2H), 7.21 (dd, J = 9.0, 2.9 Hz, 1 H), 7.52 (d, J = 2.9 Hz, 1H), 7.63 (d, J = 9.0 Hz, 1H), 7.78–7.83 (m, 2H), 8.54 (s, 1H). ^{13}C NMR (151 MHz, DMSO-d_6) δ 55.6, 102.3, 105.4, 113.6 (2C), 119.2, 120.2, 120.9 (2C), 121.5, 129.9, 130.0, 137.6, 142.0, 145.6, 157.3, 160.6. HR-MS: calculated [$C_{17}H_{15}N_4O_2^+$]: 307.1190; found [$C_{17}H_{15}N_4O_2^+$]: 307.1196 (diff.: −2.21 ppm). TLC (5% MeOH in CH_2Cl_2): R_f = 0.25. M.p.: decomposes > 300 °C. HPLC: t_R = 3.82 min (96.6% purity).

RESULTS

Molecular docking of CGS-8216. As a first step in our workflow to identify the PQ binding mode we docked the highly potent CGS-8216[24] (cpd **1**, Figure 1D) into the BZ-site of an $\alpha1\beta3\gamma2$ $GABA_A$ receptor homology model[40] , using flexible side chains as well as soft potentials on the tip of the flexible loop C (Figure 1C) (see Methods). The 100 best scored and minimized CGS-8216 docking poses (p_1 - p_{100}) were used for further evaluation.

Structure-Activity Relationship of PQ (PQ-SAR). Based on the differentiated pool of SAR data for the PQs we deduced a model which shows in the substitution positions R^5, R^6 and $R^{4'}$ a discontinuous SAR with activity cliffs while at positions R^8 and R^9 a continuous SAR is observed (Figure 2 top). In detail, it has been shown that the introduction of substituents at position R^6 leads to a dramatic loss of potency as the substituent's van-der-Waals volume increases (Figure S4). For instance, the potency of the $R^6 = CF_3$ analogue[29] (**2**, Figure 2 bottom) drops by nearly 4 orders of magnitude compared to the unsubstituted scaffold (**1**). Another considerable loss was described in the $R^5 = CH_3$ analogue **4**. The disruption of either a hydrogen bond or the introduction of a steric clash by the additional methyl group might account to the drop of more than 2 log units in potency[23]. Interestingly, analogue **5** ($R^8 = OCF_3$, $R^{4'} = COOH$) showed another dramatic potency cliff with IC_{50} = 3200 nM, whereas its amino analogue 10 ($R^8 = OCF_3$, $R^{4'} = NH_2$) remains highly potent with an IC_{50}= 0.80 nM. The drop might derive from strong electrostatic repulsion between the carboxylate group in position $R^{4'}$ and the surrounding binding pocket.

In contrast to the rugged, discontinuous SAR landscape found at positions R^5, R^6 and $R^{4'}$, at positions R^8 and R^9 large structural changes have minimal influences on compound potency (Figure 2 bottom). For example, the R^8 = *tert*-butyl, $R^{8,9}$ = benzofused and $R^{7,8}$ = methylenedioxo analogues[23,73] (**6-8**) remain highly potent despite their large and rigid substituents.

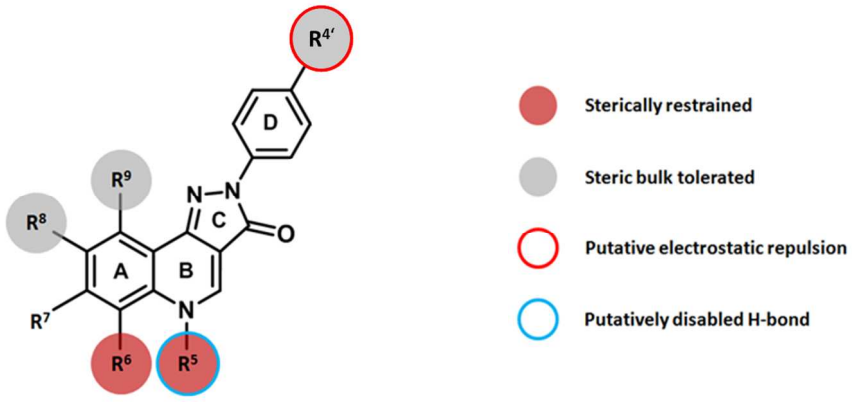

	cpd	ref	R^5	R^6	R^7	R^8	R^9	$R^{4'}$	potency (nM)	
	1	Savini et al. [23]	H	H	H	H	H	H	IC_{50} =	0.4
weak binders	**2**	Savini et al. [29]	H	CF_3	H	H	H	H	IC_{50} =	1860
	3	Savini et al. [23]	H	6,7-benzofused		H	H	H	IC_{50} >	1000
	4	Savini et al. [23]	CH_3	H	H	H	H	H	IC_{50} =	1600
	5	Savini et al. [23]	H	H	H	OCF_3	H	COOH	IC_{50} =	3200
strong binders	**6**	He at al. [73]	H	H	H	*t*Bu	H	H	K_i =	0.1
	7	Savini et al.[23]	H	H	H	8,9-benzofused		H	IC_{50} =	7.2
	8	Anathan et al. [74]	H	H	7,8-OCH_2O		H	H	IC_{50} =	3.0
	9	He at al. [73]	H	H	H	H	H	$C{\equiv}CCH_3$	K_i =	2.0
	10	Savini et al. [29]	H	H	H	OCF_3	H	NH_2	IC_{50} =	0.8

Figure 2. Top: 2D representation of PQ-SARs. The letters A, B, C and D refer to the different rings in the scaffold. The different positions and numbering of the different residues are shown by R^5-R^9 and $R^{4'}$ respectively. Positions which tolerate steric bulk (R^8, R^9 and $R^{4'}$) are indicated by gray spheres, whereas positions which do not tolerate steric bulk (R^6) are indicated by red spheres. Electrostatic repulsion is indicated by a red outline and prevented H-bond formation by a light blue outline. Bottom: table of the chemical structures and $\alpha1\beta3\gamma2$ $GABA_A$ binding affinities of PQ cpds **1-10.**

SAR guided pose selection protocol. The correct CGS-8216 binding mode should align with the PQ-SAR (Figure 2 top). Thus, we selected a set of 4 weak and 4 strong PQ binders (**2-9**, Figure 2 bottom) that reflect the essentials of the PQ-SARs. The correct binding mode should provide a rationale for the

observed potency differences within these eight analogues. In detail, the binding orientation should align with the concepts of i) steric hindrance at position R^6 (**2** and **3**), ii) steric hindrance or loss of hydrogen bonding in position R^5 (**4**), iii) high affinity despite bulky substituents at position R^8, R^9 and $R^{4'}$ (**6**-**9**) and iv) negative electrostatic repulsion at position 4' (**9** and **10**).

Considering the current difficulties of docking into homology models, we extended the conventional docking by developing a protocol which evaluates docking poses for their agreement with PQ-SAR, in an automated manner. In the first, preparatory step, the *post-docking derivatization* tool, symbolized by ">>" in the following, takes the 3D coordinates of each retrieved CGS-8216 (**1**) docking pose (p_1-p_{100}) and adds substituents to the PQ scaffold leading to post-docking derivatized protein-ligand complexes of analogues **2**-**9**. Figure 3 displays the output of the derivatization tool for **2**, **4** and **9** on docking pose p_{88}, resulting in the engineered complexes p_{88}*>>cpd 2*, p_{88}*>>cpd 4* and p_{88}*>>cpd 9*.

In the second, evaluative step, we defined a SAR scoring function which assesses the derivatized analogue placements of a particular pose (p_i***>>cpd 2-9***) for agreement with the PQ-SAR (Figure S1). The input of the $SAR_{Scoring}$ function takes calculated clash energies, H-bond interaction strength energies and distance calculations of analogues **2**-**9** as its input. For each analogue that aligns with the PQ-SAR, the function adds one point to the SAR_{Score}, resulting in a maximum score of eight points for a given pose. For a detailed description of this method we refer to the Methods section.

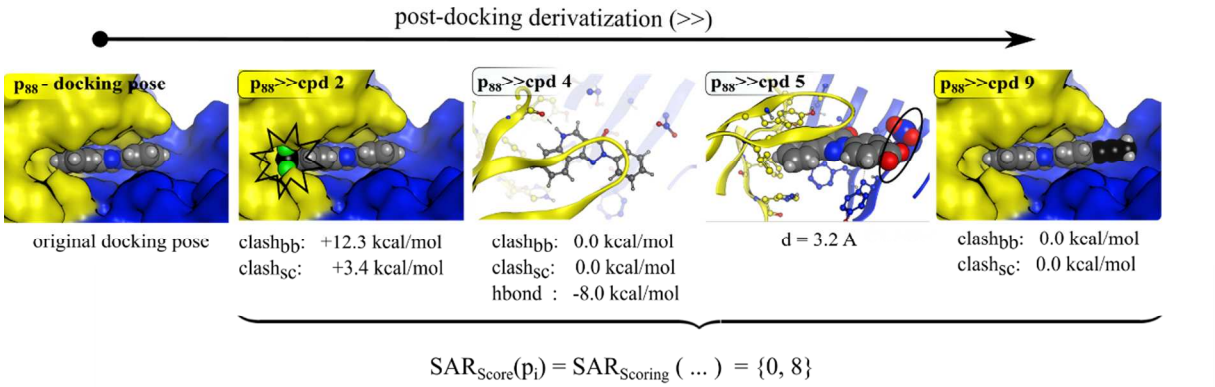

Figure 3. Post-docking derivatization and PQ analogue assessment. Original CGS-8216 docking pose p_{88} and its post-docking derivatized analogue placements *p_{88}>>cpd 2*, *p_{88}>>cpd 4*, *p_{88}>>cpd 5* and *p_{88}>>cpd 9*. Clash energy ($clash_{sc}$, $clash_{bb}$), interatomic distances (d) and hydrogen bond strength interactions (h_{bond}) were calculated and serve as input for the SAR scoring function (see Methods and Figure S1). For each analogue that aligns with the PQ-SAR (Figure 2 top) one point is added to the SAR_{Score} of a particular pose, leading to a maximum SAR_{Score} of eight. yellow, α1 subunit; blue, γ2 subunit; black space-filling atoms, carbon atoms introduced in the post-docking derivatization step; $clash_{bb}$, ligand clashes with backbone and C_β atoms; $clash_{sc}$, ligand clashes with sidechain atoms; d, shortest distance between *p_i>>cpd 5* carboxylate group atoms and an ASP/GLU carboxylate group atoms; h_{bond}, H-bond interaction strength between quinolone nitrogen and binding pocket (see Methods).

SAR scoring function identifies two candidate binding modes. To obtain an overview of the geometric heterogeneity of the 100 CGS-8216 docking poses, we applied multidimensional scaling (MDS) methodology on the basis of the ligand RMSD distance matrix (see Methods). Docking poses which are in vicinity to each other in the MDS plot share a similar binding mode (BM) while dissimilar poses are distant to each other (Figure 4A). The MDS plot showed a Kruksal-Stress of 0.19[75] which is sufficient for visualization purpose. SAR assessment of 100 poses resulted in 14 poses with a SAR_{Score} greater than 6 (Table S2). These poses can be grouped into two geometrically different binding modes, BM I (Figure 4B) and BM II (Figure 4C). Twelve of the 14 best SAR scored poses belonged to BM I,

containing two poses with the maximum SAR_{Score} of 8. The remaining two poses belonged to BM II, with best score of 6 (Table S2, Figure S5).

The main geometric difference between BM I and BM II is the orientation of the CGS-8216's D ring. In BM I, the carbonyl oxygen and the D ring point both to the γ2 subunit, while in BM II, they point towards the α1 subunit. With respect to the interaction profiles of BM I and BM II, we found similar interactions of their A and B rings. In both binding orientations the quinoline nitrogen (N5) is engaged in H-bond interactions with the backbone of α1Y159, while γ2F77 and α1Y209 show hydrophobic and/or π–π interactions with the quinoline ring. In contrast, the interactions and position of the D ring differ significantly. In BM I, the D-ring showed strong interactions with γ2Y58 and is pointing towards the F-loop (Figure 4B). In BM II it mainly interacts with α1H101 and is located close to loop B of the α subunit (Figure 4C).

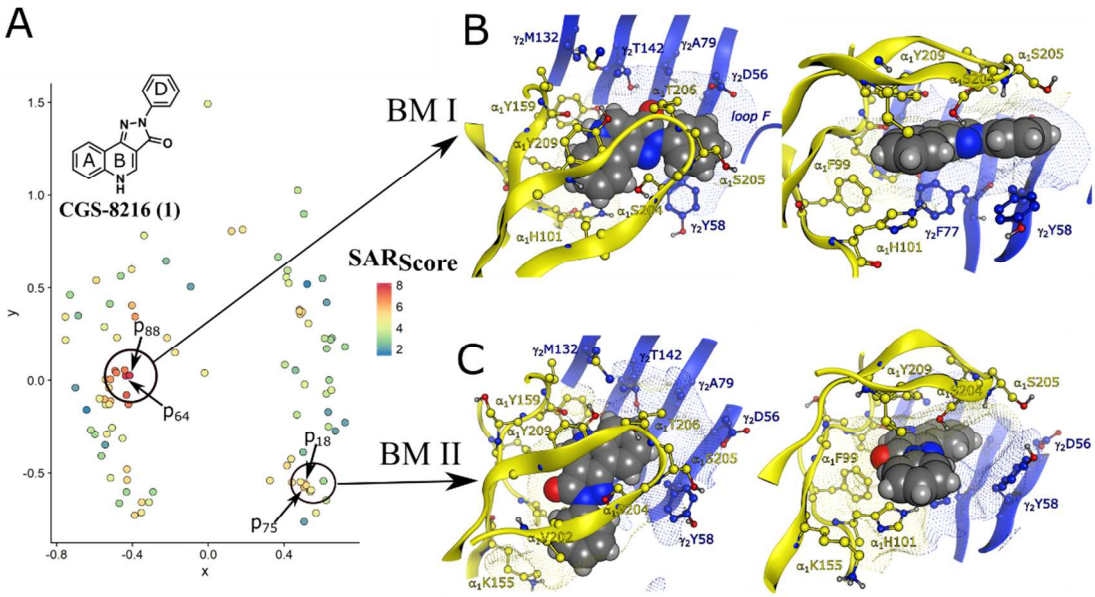

Figure 4. Identification of two major binding modes BM I and BM II. (A) Visualization of the CGS-8216 pose space utilizing MDS (see Methods, Figure S5). The color of the dots reflects the agreement of these poses with the SAR scoring from blue (low agreement) to red (high agreement). In the left center of the MDS plot, a cluster of highly scored poses, containing two poses with a maximum SAR_{Score} of 8, was found. These poses were defined as BM I. A second group of poses, in the lower right corner of the MDS plot, showed a moderate score of 6. All other poses had a SAR_{Score} below 6

points. A 2D representation of CGS-8216 can be found in the upper left corner, with its rings labeled. (B) Top and side view of the representative BM I pose p_{88}, with the side chain rotamers as seen in this particular pose. (C) Top and side view of the representative BM II p_{18}, with the side chain rotamers as seen in this particular pose. It should be noted that side chain rotamers cannot be predicted reliably from homology models at this level of sequence similarity. yellow, α1 subunit; blue, γ2 subunit

Analysis of BM I and BM II in the light of PQ-SAR. Two BM I poses (p_{88} and p_{64}) displayed the maximum SAR_{Score} of 8 and perfectly fit the PQ-SAR. For characterizing BM I we selected p_{88} (Figure 5A) and its derivatized analogue placements, *p_{88}>>cpds 2-9* (Figure 5B). The low potency of **2**-**5** is well reflected in the p_{88}. The derivatized placements *p_{88}>>cpds 2-3* displayed severe backbone clashes with α1Y159 and α1S158, congruent with the dramatic potency drop seen in R^6 substituted analogues (Figure S4). The strong H-bond interaction between the quinolone nitrogen and the carbonyl oxygen of α1Y159 in p_{88} aligns with the low potency of the N-methylated analogue **4**. The carboxylate group of the D-ring in *p_{88}>>cpd 5* was found to be close to γ2D56 and points towards loop F, on which γ2E189 and γ2D192 are positioned (Figure S6). This orientation is in good agreement with analogue's **5** low potency. Finally, post-engineered placements for the highly active, bulky R^8 = tertbuyl, $R^{8,9}$ = benzofused, $R^{7,8}$ = OCH_2O and $R^{4'}$ = $C{\equiv}CCH_3$ (**6-9**) analogues (*p_{88}>>cpds 6-9)* showed minor to no clashes. Substitution sites R^8 and R^9, though still in the pocket already point towards the pocket entry and bulk water. CGS-8216's ring D was placed below the tip of loop C and is partly solvent exposed. Thus, analogue **9** with its rigid and bulky -$C{\equiv}CCH_3$ substituent at $R^{4'}$ fits well into the pocket.

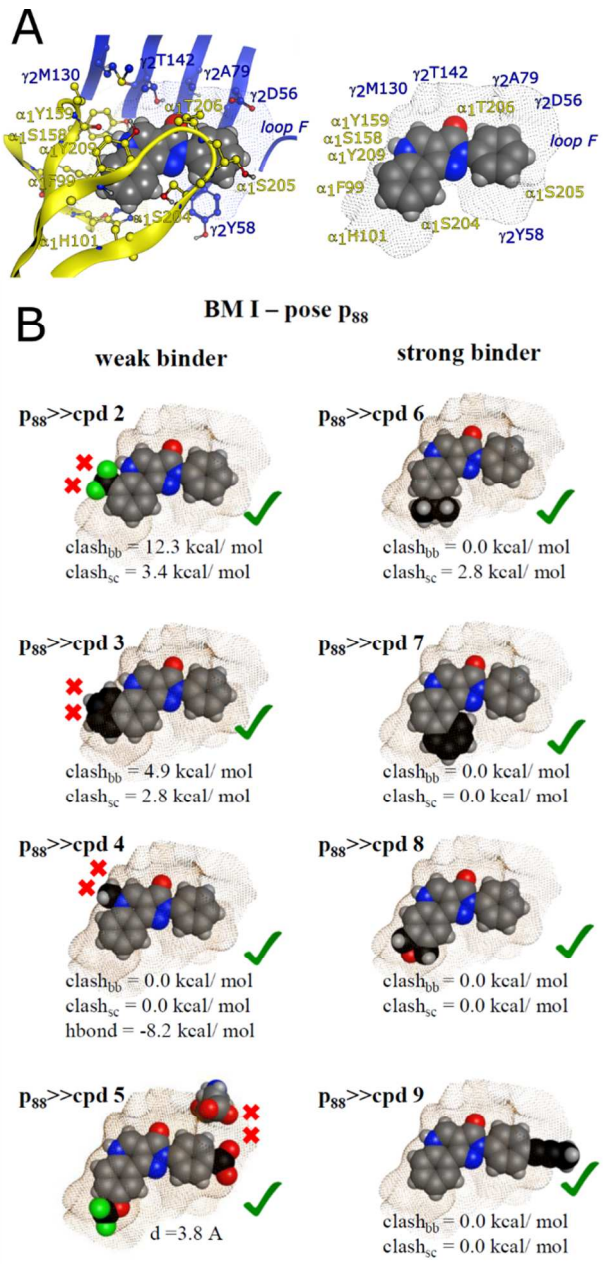

Figure 5: BM I in the light of the PQ-SAR model. (A) Homology model of the high affinity binding site at the extracellular α1+/γ2− interface showing p_{88} in BM I orientation (α1 subunit = yellow, γ2 subunit = blue, pocket surface = gold grid). Focused perspective of the ligand orientation in the pocket surface grid. (B) Table of weak and strong PQ binders in BM I orientation. Agreement of the derivatized *p_{88}>>cpd 2-9* with the PQ-SAR (Figure 2) is displayed by green hooks. Unfavorable interactions such as and putative electrostatic repulsion or steric clashes are displayed by red crosses. black space-filling atoms, carbon atoms introduced in the post-docking derivatization step (Figure 3); $clash_{bb}$, ligand clashes with backbone and C_β atoms; $clash_{sc}$, ligand clashes with sidechain atoms; d,

shortest distance between p_i*>>cpd 5* carboxylate group and an ASP/GLU carboxylate group; h_{bond}, H-bond interaction strength between quinolone nitrogen and binding pocket (see Methods).

The best BM II pose displayed a SAR_{Score} of 6 and hence could not fully explain the PQ-SAR. For characterizing BM II we selected p_{18} (Figure S7) and its derivatized analogue placements, p_{18}*>>cpds 2-9***.** In p_{18}*>>cpds 2-3* we found severe clashes with the side chain atoms of γ2M130 and γ2T142. Likewise, to BM I, the quinoline nitrogen showed hydrogen bond interaction with the backbone carbonyl oxygen of α1Y159. Hence, the potency loss seen in p_{18}*>>cpd 4* is plausible as well.

In contrast to BM I, BM II fails to provide a rationale for the dramatic loss in affinity seen in the carboxy analogue **5**. Among the closest residues to p_{18}*>>cpd 5* carboxyl group were the weak and strong basic amino acids, α1H101 and α1K155 (Figure 4C). The vicinity of these basic amino acids to ring D in p_{18}*>>cpd 5* is in contradiction to the assumption of strong negative electrostatic repulsion between the analogue **5**'s carboxylate moiety and the pocket environment. Finally, the four active analogues **6-9** are well represented in BM II by *p1>>cpds 6-9* (Figure S7).

Stability and affinity evaluation of 5 and 10 in BM I and BM II. BM I is in agreement with the PQ-SAR, while BM II fails to provide a rational for the poor activity of **5**. To investigate this further additional analyses were conducted. We used the post-docking derivatized complexes of analogues **5** and **10** for the best scored BM I (p_{64} and p_{88}) as well as the BM II (p_{18} and p_{75}) poses (Table S2, Figure S5) to investigate the stability of the ligands using MD simulations and employing simple RMSD criteria[76]. Additionally, the difference in relative binding free energy for **5** and **10** in BM I and BM II was calculated.

The stability of the selected poses was evaluated using an adopted validation scheme described by Liu *et al.*[76]. Ten independent MD simulations (same coordinates but different initial velocities) were conducted for the derivatized BM I (p_{64}*>>cpd 5*, p_{64}*>>cpd 10*, p_{88}*>>cpd 5*, p_{88}*>>cpd 10*) and BM II

(p_{18}>>*cpd 5*, p_{18}>>*cpd 10*, p_{75}>>*cpd 5*, p_{75}>>*cpd 10*) placements. To distinguish between stable and unstable poses we considered the average ligand-RMSD of the ten MD simulations (<L-RMSD>) and the number of MD simulations with a L-RMSD below 2 Å (Table 1 and Table S3). In addition to the geometric analysis the free energy differences of each p_i>>*cpd 5* - p_i>>*cpd 10* pair were calculated (Figure S2-S3 and Table S1).

Table 1. MD-based stability analysis and interaction profile of **5** and **10** in BM I and BM II, respectively (Figure S8- S9).

	cpd **5** ($R^{4'}$ = COOH)				cpd **10** ($R^{4'}$ = NH_2)			
	BM I		BM II		BM I		BM II	
	p_{88}	p_{64}	p_{18}	p_{75}	p_{88}	p_{64}	p_{18}	p_{75}
<L-RMSD[a]>	2.3	2.6	1.7	1.9	1.5	1.7	2.4	2.6
< 2.0 Å[b] >	7/10	2/10	8/10	7/10	10/10	8/10	3/10	2/10
AB-ring[c]	α1F99, α1H101, α1V202, α1Y209, γ2F77		γ2F77, α1Y209		α1F99, α1H101, α1V202, α1Y209, γ2F77		α1Y159, α1Y209, γ2F77	
N5-nitrogen[d]	-		-		α1Y159		-	
C-ring[d]	α1S204, γ2T142		-		α1S204, γ2T142		-	
D-ring[c]	γ2Y58		α1V202, γ2Y58, α1H101		γ2Y58		α1V202, γ2Y58, α1H101, α1F99	
Position $R^{4'}$: $COOH/NH_2$[e]	γ2K184, γ2R194		α1K155, γ2R194, γ2R197		γ2D56		-	

[a] average L-RMSD of 10 independent MD simulations.
[b] Number of MD simulations for which the L-RMSD was below 2.0 Å
[c] Hydrophobic and aromatic interactions.
[d] Hydrogen bond interactions.
[e] Ionic interactions.

First, the stability and relative free energy difference for cpd **5** and **10** in BM I (p_{64} and p_{88}) was evaluated. For cpd **10** the <L-RMSD> values for the 10 MD simulations are 1.5 Å in p_{88} and 1.7 Å in p_{64} suggesting an overall stable complex for BM I, which is additionally reflected by the number of simulations with an L-RMSD below 2 Å (18 out of 20 for both poses). For cpd **5** we obtained

ambiguous results even though the <L-RMSD> of 2.3 Å in p_{88} and 2.6 Å in p_{64} are above the stability criteria and thus suggesting a low stability of **5**. However, considering the simulations in p_{88} we observed only three simulations with an L-RMSD higher than 2 Å (L-RMSD between 4.3 Å and 5.6 Å) putting this quantitative analysis in doubt. The relative binding free energy difference between **5** and **10** in BM I was calculated as -2.5 kcal/mol (standard deviation of 1.3 kcal/mol) reflecting the higher affinity of **10**. The proximity between the carboxylic group of **5** and γ2D56 seemingly leads to a destabilization of the binding pose in BM I.

Interestingly, in BM II a contrary stability profile for **5** and **10** (p_{18} and p_{75}) was observed. For **5** <L-RMSD> values of 1.7 Å in p_{18} and 1.9 Å in p_{75} were obtained and the majority of the individual MD simulations were below 2.0 Å indicating a high stability of **5** in BM II. In contrast, **10** displayed <L-RMSD> values of 2.4 Å in p_{18} and 2.6 Å in p_4. In addition, most individual simulations (15 out of 20 simulations) showed L-RMSD values higher than 2.0 Å suggesting a low stability of **10** in BM II. Moreover, the calculated difference in binding free energy between **5** and **10** is 0.02 kcal/mol (standard deviation of 1.88 kcal/mol). These results provide further evidence against BM II as it failed to rationalize the difference in potency between **5** and **10**.

SAR guided docking vs. conventional molecular docking protocols – a comparison. We were interested whether conventional docking protocols would favor a similar binding mode (BM I) as our new SAR-driven protocol. For this purpose, we conducted molecular docking using six different docking protocols. We performed flexible docking of CGS-8216 into our α1β3γ2 $GABA_A$ homology model utilizing MOE 2013.08[45], GOLD 5.2[43], Schrödinger's Induced Fit[66] and AutoDock Vina 1.1.220[67]. The poses within each run were ranked by the software's internal scoring function encompassing the GBVI/WSA dG[65], London dG[64], ChemScore[46], GoldScore[46], Glide SP[77] and the AutoDock Vina scoring function[67]. We kept the best scored pose per scoring function and compared these orientations against p_{88} (BM I) from the SAR guided protocol. While AutoDock Vina (RMSD ~ 1.5 Å) and Induced Fit protocol (RMDS ~ 2.8 Å) were able to identify similar binding modes as our

SAR guided protocol, the other four protocols showed completely different orientations with RMSD distances greater than 6 Å (Table S4).

Prospective γ2D56A mutant strengthens BM I binding hypothesis. Based on the conclusive results of our *in silico* analysis we aimed to strengthen our binding hypothesis (BM I) by a prospective mutation. In BM I, CGS-8216's pending phenyl ring is in the vicinity to three acidic residues, γ2D56, γ2E189 and γ2D192 (Figure S6). We selected the residue closest to CGS-8216 in BM I, γ2D56 and converted it into an alanine residue (γ2D56A). This point mutation should lead to a loss of the putative electrostatic repulsion feature of our previous analysis (Figure 2). To address this missing feature we synthesized two ligands, namely compound **18** and **19**, which differ from **5** and **10** only in the position R^8 (for **18** and **19** $R^8 = OCH_3$; for **5** and **10** $R^8 = OCF_3$) while possessing the same electrostatic properties in position $R^{4'}$ (Scheme 1). Converting the 4-methoxyaniline with diethylethoxymethylene malonate *via* the Gould-Jacobs[78] reaction yielded the quinoline **14**. Treatment with $POCl_3$ led to **15** which was reacted further with 4-nitrophenylhydrazine and 4-cyanophenylhydrazine respectively to obtain the precursors **16** and **17**. The reduction of **16** yielded the desired amine **18** and basic hydrolysis of **17** led to the corresponding carboxylic acid derivative **19** (Scheme 1).

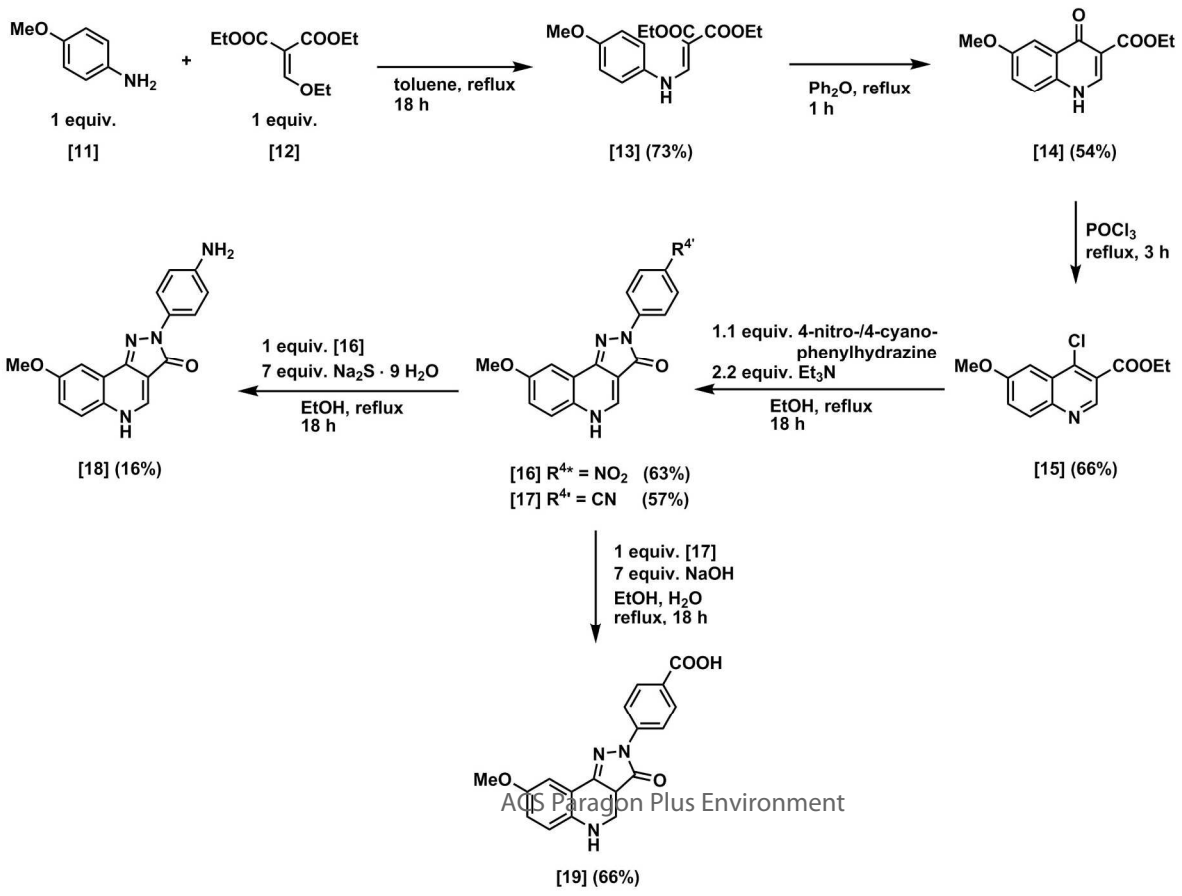

Scheme 1. Synthetic route to compound **18** and **19**.

First, we tested our new PQ ligands in α1β3γ2 wild type receptors to verify that **19** with the carboxylic acid moiety in position $R^{4'}$ is a weak binder compared to **18** with the amino group in the same position. As expected **18** (K_i = 0.21 ± 0.03 nM) displayed a three order of magnitude higher potency compared to **19** (K_i = 161 ± 27 nM) (Figure 6, grey lines). Thus, we were able to investigate our new compounds in the α1β3γ2-D56A mutant construct. Remarkably, we observed for **19** an increase of potency by a factor of higher than 10 (K_i = 15 ± 2 nM) due to the introduction of our single point mutation whereas **18** showed only a very weak potency shift by a factor of 2 (K_i = 0.094 ± 0.005 nM) (Figure 6, dotted lines). Hence, these results support our binding hypothesis that PQs favor BM I.

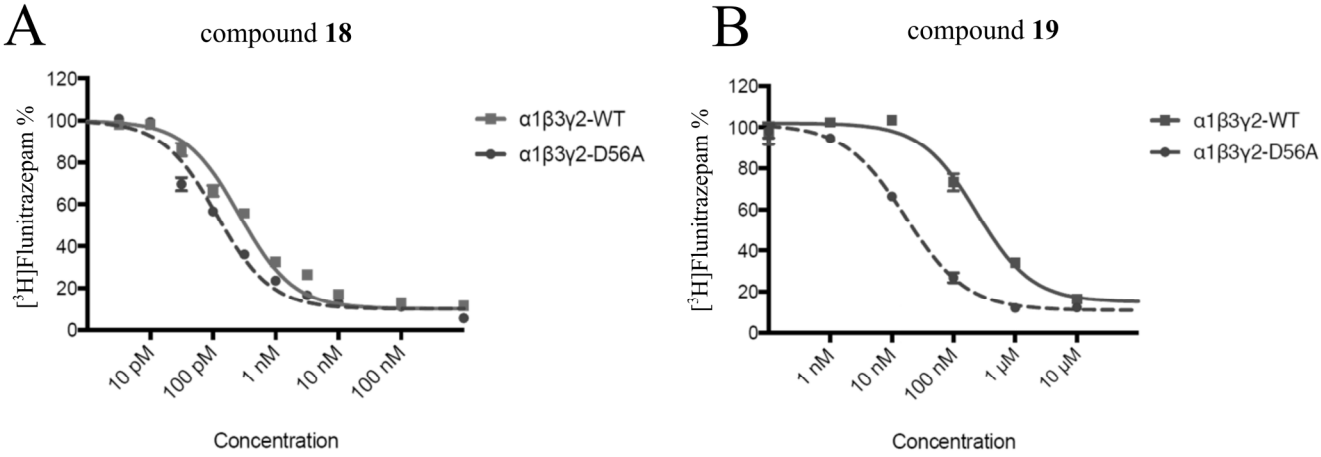

Figure 6: (A) [^{3}H]Flunitrazepam displacement assay of **18** in α1β3γ2-WT receptors (■, K_i = 0.21 ± 0.03 nM) and α1β3γ2S-D56A mutants (●, K_i = 0.094 ± 0.005 nM) (mean ± SEM, n = 3-4). (B) [^{3}H]Flunitrazepam displacement assay of **19** in α1β3γ2S-WT receptors (■, K_i = 161 ± 27 nM) and α1β3γ2S-D56A mutants (●, K_i = 15 ± 2 nM) (mean ± SEM, n = 3-4). Drug concentrations resulting in half maximal inhibition of specific [^{3}H]Flunitrazepam binding (IC_{50}) were converted to K_i values by using the Cheng-Prusoff relationship (Figure S10).

DISCUSSION

The experimental elucidation of drug-target complexes is labor-intensive and even impossible for many membrane-bound drug targets. Here, computational approaches such as homology modeling combined with molecular docking can generate reasonable binding hypotheses, but frequently docking scoring functions struggle to filter them from a pool of alternative orientations[9].

To increase the credibility of docking pose selection for low-reliability target structures, we established in this study a fully automatized routine applicable to molecules for which a distinct SAR is available. Specifically, we defined a docking scoring function that solely evaluates docking poses by their degree of SAR agreement. To evaluate binding orientations, we derived analogue placements from four weak (**2-5**) and four strong (**6-9**) binders (Figure 2 bottom) on the basis of the coordinates of each CGS-8216 docking pose (Figure 3). Subsequently, the SAR scoring function utilized clash analysis, distance calculation and H-bond interaction strength calculation to assess the congruence between the analogue placement and the PQ-SAR (see Methods and Figure S1).

Our SAR-driven docking protocol led to one favorable binding mode, BM I (Figure 4B), fully compatible with the PQ-SAR (Figure 5B), reflected by a maximum SAR_{Score} of eight. A second, moderately performing binding mode, BM II (Figure 4C), failed to provide a structural evidence for the assumed electrostatic repulsion between carboxy analogue (**5**) and the pocket environment (Figure S6). However, the SAR scoring function estimates the electrostatic repulsion assumption by simple distance calculations (see Methods).

To evaluate the electrostatic influence more sophisticatedly, we performed MD based stability analysis for the two best SAR scored BM I and BM II poses and relative binding free energy calculations for the carboxy analogue (**5**) and the amino analogue (**10**) in each binding mode. In BM I the results of the relative binding free energy calculations as well as the stability analysis indicate that **10** is stable in contrast to **5** – thus BM I can give a rationale for the reported potency discrepancy between these analogues while BM II failed. Here, **10** is more stable than **5** and there is no difference in the relative binding free energy between **5** and **10**.

In total, our protocol led to one convincing CGS-8216 binding mode (BM I) providing a structural rationality for the PQ-SAR (Figure 5B). In BM I, the A and B ring, both show strong hydrophobic and π–π interactions with α1F99, α1Y209 and γ2F77 (Figure 4B). The importance of γ2F77 for PQ binding was shown in the γ2F77I mutant which led to a 10-fold drop in potency for CGS-8216's methoxy analogue CGS-9895[79]. Our MD simulations indicate that CGS-8216's ring C is involved in H-bond interaction with α1S204 as well as γ2T142. Finally, the pending phenyl ring D shows strong hydrophobic interactions with γ2Y58 and is located close to the acidic residues γ2D56, γ2E189 and γ2D192 (Figure S6).

To provide experimental evidence for BM I we designed an experiment which reduced the negative electrostatic potential of the protein environment close to CGS-8216's D ring. The reduction in negative potential was introduced by the γ2D56A point mutation and in fact, the synthesized CGS-8216's carboxy analogue (**19**) showed a 10-fold increase in potency in the γ2D56A mutant compared to the α1β3γ2 $GABA_A$ receptor wild type while its amino analogue (**18**) was only influence by a factor of 2 (Figure 6).

Lastly, we compared the result of our SAR-driven docking routine with the output from conventional docking protocols. In two out of six protocols, we found solutions that come close to BM I (RMSD < 3 Å) (Table S4) while the others show completely different orientations (RMSD > 6 Å). The observed variety in docking outputs derived from different protocols may reflect the current difficulty of molecular docking into homology models[10]. However, it has to be stated that the docking protocols used in the comparison were selected by the authors' availability and did not result from prior protocol-target assessment [80]. A remarkable study in the predicton of scaffold binding modes by ligand based knowledge has been carried out at the αβ-tubulin colchicine site[81]. Here, Chenxiao et *al.* combined ensemble docking of analogue series to infer 3D-QSAR models eventually utilized for binding hypothesis evaluation. In contrast to our study, the early selection of docking poses was influenced by an energetic scoring function[82].

The inferred CGS-8216 binding mode might pave the way to improved antagonists from either the PQ chemotype itself or by scaffold hopping to new chemotypes. Furthermore, the binding orientation can provide important information to guide ADME optimization. Lead optimization of PQ was impeded, among other factors, by the poor solubility of this compound class[25]. The binding mode can be utilized to select the optimal substitution site for the introduction of water-solubilizing groups, such as morpholine, piperazine and tertiary amine moieties, that do not compromise potency[83]. From BM I perspective, potential sites for these positively-ionizable groups are the *meta* and *para* positions of PQ's D-ring, as they point towards the bulk solvent and would be embedded in an electronegative environment shaped by γ2D56, γ2E189 and γ2D192 (Figure S6). In this respect, the finding of Savini et al.[84] that meta-NH_2 substitutions increase PQs potencies fits well with our proposal. In BM I (Figure 4B), the meta-position of ring D is pointing directly towards γ2D56. Hence, H-bond donating substituents on the meta position, like the meta–NH_2 moiety, could form favorable hydrogen bond interactions with the acidic residue, and would agree with the observed potency increase (Figure S11).

Ultimately, this could accelerate the quest to find urgently required benzodiazepine site antagonists with novel *in vitro* and *in vivo* profile, such as compounds for oral administration.

One drawback of our SAR-driven protocol, at its current stage, is the neglect of mutual structural adaptation of both ligand and receptor as response to substituent introduction in the post-docking derivatization step (Figure 3). We partly compensated the rigid perspective by introducing clash thresholds and distinguishing between backbone and sidechain clashes (Figure S1). While these considerations sufficed to lead to one consistent CGS binding mode, it might be inappropriate in other scenarios. Hence, a more sophisticated representation of induced fit phenomena in the SAR-driven docking protocol by e.g. the inclusion of energy minimization, appears to be a reasonable advancement in future studies.

The starting point of our study, low-reliability in protein structural information on the one hand and SAR knowledge on the other hand is common for many scaffolds binding to membrane-bound drug targets. For example, 800 000 bioactivity endpoints, amenable to SAR deduction, are deposited in the

publicly available ChEMBL 23 database[85] for the important drug target class of GPCRs. However, next to SAR availability, the applicability of our protocol strongly depends on the characteristics and the quality of the underlying SAR. Incongruent SAR patterns as well as an inadequate SAR-hypersurface impede the presented approach. For example, a flat SAR without any discontinuity[30] would not carry any discriminative potential for pose prioritization. Here, calculation of the SAR Index[86] might provide a fast suitability assessment. In terms of target space, we assume that due to the stiffness of the post-docking derivatization procedure (Figure 3), our protocol might be more applicable on proteins accommodating rather rigid binding pockets. Hence, in addition to SAR Index calculation[86], B-factor analysis[87] and algorithms to assess protein flexibility[88] provide estimates for the suitability of our protocol at a given context.

In summary, in this study we introduced a protocol that increases the credibility of docking pose selection for targets with low structural reliability. We established this by an automatized routine applicable to molecules for which a distinct SAR is available. The routine was complemented by elaborate MD simulations, composed of relative binding free energy calculations and stability assessment on a preselected set of poses with high SAR congruency. The presented approach in binding mode prediction can be expanded to other drug targets with a similar profile in terms of target structure uncertainty and SAR availability as found in $GABA_A$ receptors, such as GPCRs.

ASSOCIATED CONTENT

Supporting Information

The Supporting information and Chemical Compound Information is available free of charge on the ACS Publication website.

Formula and components of the SAR scoring function; SAR Score decomposition of top ranked CGS-8216 docking poses; Outcome of convential docking protocols; More details of settings and outcomes of MD and FES analysis; Compound characterization (1H NMR, 13C NMR and HPLC of compounds **17-19** (PDF)

Results (in kcal/ mol) of FES (XLSX)

Molecular formula strings (CSV)

AUTHOR INFORMATION

Corresponding author

*Phone: +43(1)427755113. E-mail: lars.richter@univie.ac.at.

ORCID

Lars Richter: 0000-0002-9417-9042

Author Contributions

‡D.C.B.S. and M.W. contributed equally to this study. L.R., G.E., M.E., M.W., and D.C.B.S. participated in the design of the research. Molecular docking studies were conducted by L.R., L.S. and

D.C.B.S. Chemical synthesis was designed and conducted by D.C.B.S., M.D.M., M.S. Radioligand displacment assays were performed by P.S. MD simulations and FES simulations were designed and conducted by M.W., T.L. and S.B. All authors wrote or contributed to the writing of the manuscript. All authors contributed to writing the manuscript.

Notes

The authors declare no competing financial interest.

ACKNOWLEDGEMENT

This work was financially supported by Austrian Science Fund grants W1232 (graduate school program MolTag for D. C. B. S.) and P27746.

ABBREVIATIONS USED

PQ, pyrazoloquinolinone, SAR; structure-activity relationship; MD, molecular dynamics; FES, free energy simulations; D3R, Drug Design Data Resource; BZ, benzodiazepines; RMSD, root mean square deviation; BM, binding mode; L-RMSD, ligand-RMSD

REFERENCES

(1) Greer, J.; Erickson, J. W.; Baldwin, J. J.; Varney, M. D. Application of the Three-Dimensional Structures of Protein Target Molecules in Structure-Based Drug Design. *J. Med. Chem.* **1994**, *37*, 1035–1054.

(2) Maddaford, S. P. A Medicinal Chemistry Perspective on Structure-Based Drug Design and Development. *Methods Mol. Biol.* **2012**, *841*, 351–381.

(3) Warne, T.; Moukhametzianov, R.; Baker, J. G.; Nehmé, R.; Edwards, P. C.; Leslie, A. G. W.; Schertler, G. F. X.; Tate, C. G. The Structural Basis for Agonist and Partial Agonist Action on a B1-Adrenergic Receptor. *Nature* **2011**, *469*, 241–245.

(4) Grey, J. L.; Thompson, D. H. Challenges and Opportunities for New Protein Crystallization Strategies in Structure-Based Drug Design. *Expert Opin. Drug Discov.* **2010**, *5*, 1039–1045.

(5) Schmidt, T.; Bergner, A.; Schwede, T. Modelling Three-Dimensional Protein Structures for Applications in Drug Design. *Drug Discov. Today* **2014**, *19*, 890–897.

(6) Kubinyi, H. Similarity and Dissimilarity: A Medicinal Chemist's View. *Perspect. Drug Discov. Des.* **1998**, 225–252.

(7) Vyas, V. K.; Ukawala, R. D.; Ghate, M.; Chintha, C. Homology Modeling a Fast Tool for Drug Discovery: Current Perspectives. *Indian J. Pharm. Sci.* **2012**, *1*, 1–17.

(8) Sousa, S. F.; Ribeiro, a J. M.; Coimbra, J. T. S.; Neves, R. P. P.; Martins, S. a; Moorthy, N. S. H. N.; Fernandes, P. ; Ramos, M. J. Protein-Ligand Docking in the New Millennium--a Retrospective of 10 Years in the Field. *Curr. Med. Chem.* **2013**, *20*, 2296–2314.

(9) Jorgensen, W. L. Efficient Drug Lead Discovery and Optimization. *Acc. Chem. Res.* **2009**, *42*, 724–733.

(10) Yuriev, E.; Holien, J.; Ramsland, P. A. Improvements, Trends, and New Ideas in Molecular Docking: 2012-2013 in Review. *J. Mol. Recognit.* **2015**, *28*, 581–604.

(11) Beier, C.; Zacharias, M. Tackling the Challenges Posed by Target Flexibility in Drug Design. *Expert Opin. Drug Discov.* **2010**, *5*, 347–359.

(12) Ferreira, L.; dos Santos, R.; Oliva, G.; Andricopulo, A. Molecular Docking and Structure-Based Drug Design Strategies. *Molecules* **2015**, 20, 13384-421

(13) Straatsma, T. Computational Alchemy. *Annu. Rev. Phys. Chem.* **1992**, *43*, 407–435.

(14) Gathiaka, S.; Liu, S.; Chiu, M.; Yang, H.; Stuckey, J. A.; Kang, Y. N.; Delproposto, J.; Kubish, G.; Dunbar, J. B.; Carlson, H. A.; Burley, S.K.; Walters, W.P.; Amaro, R.E.; Feher, V.A.; Gilson, M.K. D3R Grand Challenge 2015: Evaluation of Protein–ligand Pose and Affinity Predictions. *J. Comput.-Aided. Mol. Des.* **2016**, *30*, 651–668.

(15) Gaieb, Z.; Liu, S.; Gathiaka, S.; Chiu, M.; Yang, H.; Shao, C.; Feher, V. A.; Walters, W. P.; Kuhn, B.; Rudolph, M. G.; Burley, S.K.; Gilson, M.K.; Amaro, R.E. D3R Grand Challenge 2: Blind Prediction of Protein–ligand Poses, Affinity Rankings, and Relative Binding Free Energies. *J. Comput.-Aided. Mol. Des.* **2017**, *32*, 1–20.

(16) Sieghart, W. Allosteric Modulation of GABAA receptors via Multiple Drug-Binding Sites. In *Advances in Pharmacology*; **2015**, 72, pp 53–96.

(17) Olsen, R.; Sieghart, W. International Union of Pharmacology. LXX. Subtypes of Gamma-Aminobutyric Acid A Receptors: Classification on the Basis of Subunit Structure and Receptor Function. *Pharmacol. Rev.* **2008**, *60*, 243–260.

(18) Sigel, E. Mapping of the Benzodiazepine Recognition Site on GABA(A) Receptors. *Curr. Top. Med. Chem.* **2002**, *2*, 833–839.

(19) Skolnick, P. Anxioselective Anxiolytics: On a Quest for the Holy Grail. *Trends Pharmacol. Sci.* **2012**, *33*, 611–620.

(20) Clayton, T.; Chen, J. L.; Ernst, M.; Richter, L.; Cromer, B. A.; Morton, C. J.; Ng, H.; Kaczorowski, C. C.; Helmstetter, F. J.; Furtmüller, R.; Ecker, G.; Parker, M.W.; Sieghart, W.; Cook, J.M. An Updated Unified Pharmacophore Model of the Benzodiazepine Binding Site on Gamma-Aminobutyric Acid(a) Receptors: Correlation with Comparative Models. *Curr. Med. Chem.* **2007**, *14*, 2755–2775.

(21) He, X.; Huang, Q.; Ma, C.; Yu, S.; McKernan, R.; Cook, J. M. Pharmacophore/Receptor Models for GABA(A)/BzR α2β3γ2, α3β3γ2 and α4β3γ2 Recombinant Subtypes. Included Volume Analysis and Comparison to α1β3γ2, α5β3γ2, and α6β3γ2 Subtypes. *Drug Des. Discovery* **2000**, *17*, 131–171.

(22) Hadjipavlou-Litina, D.; Hansch, C. Quantitative Structure–Activity Relationships of the Benzodiazepines. A Review and Reevaluation. *Chem. Rev.* **1994**, *94*, 1483–1505.

(23) Savini, L.; Chiasserini, L.; Pellerano, C.; Biggio, G.; Maciocco, E.; Serra, M.; Cinone, N.; Carrieri, A.; Altomare, C.; Carotti, A. High Affinity Central Benzodiazepine Receptor Ligands. Part 2: Quantitative Structure-Activity Relationships and Comparative Molecular Field Analysis of Pyrazolo[4,3-c]Quinolin-3-Ones. *Bioorganic Med. Chem.* **2001**, *9*, 431–444.

(24) Boast, C. A.; Snowhill, E. W.; Simke, J. P. CGS 8216 and CGS 9896, Novel Pyrazoloquinoline Benzodiazepine Ligands with Benzodiazepine Agonist and Antagonist Properties. *Pharmacol. Biochem. Behav.* **1985**, *2*, 639–644.

(25) Hirschberg, Y.; Oberle, R. L.; Ortiz, M.; Lau, H.; Markowska, M. Oral Absorption of CGS-20625, an Insoluble Drug, in Dogs and Man. *J. Pharmacokinet. Biopharm.* **1995**, *23*, 11–23.

(26) Ramerstorfer, J.; Furtmuller, R.; Sarto-Jackson, I.; Varagic, Z.; Sieghart, W.; Ernst, M. The GABAA Receptor + - Interface: A Novel Target for Subtype Selective Drugs. *J. Neurosci.* **2011**, *31*, 870–877.

(27) Varagic, Z.; Wimmer, L.; Schnürch, M.; Mihovilovic, M. D.; Huang, S.; Rallapalli, S.; Cook, J. M.; Mirheydari, P.; Ecker, G. F.; Sieghart, W.; Ernst, M. Identification of Novel Positive Allosteric Modulators and Null Modulators at the GABAA Receptor A+β- Interface. *Br. J. Pharmacol.* **2013**, *169*, 371–383.

(28) Varagic, Z.; Ramerstorfer, J.; Huang, S.; Rallapalli, S.; Sarto-Jackson, I.; Cook, J.; Sieghart, W.; Ernst, M. Subtype Selectivity of A+β- Site Ligands of GABAA Receptors: Identification of the First Highly Specific Positive Modulators at A6β2/3γ2 Receptors. *Br. J. Pharmacol.* **2013**, *169*, 384–399.

(29) Savini, L.; Massarelli, P.; Nencini, C.; Pellerano, C.; Biggio, G.; Maciocco, A.; Tuligi, G.; Carrieri, A.; Cinone, N.; Carotti, A. High Affinity Central Benzodiazepine Receptor Ligands: Synthesis and Structure–activity Relationship Studies of a New Series of Pyrazolo[4,3-c]Quinolin-3-Ones. *Bioorg. Med. Chem.* **1998**, *6*, 389–399.

(30) Eckert, H.; Bajorath, J. Molecular Similarity Analysis in Virtual Screening: Foundations, Limitations and Novel Approaches. *Drug Discov. Today* **2007**, *12*, 225–233.

(31) Anighoro, A.; Bajorath, J. Three-Dimensional Similarity in Molecular Docking: Prioritizing Ligand Poses on the Basis of Experimental Binding Modes. *J. Chem. Inf. Model.* **2016**, 56, 580-587.

(32) Kumar Ojha, P.; Mitra, I.; Kar, S.; Narayan Das, R.; Roy, K. Lead Hopping for PfDHODH Inhibitors as Antimalarials Based on Pharmacophore Mapping, Molecular Docking and Comparative Binding Energy Analysis (COMBINE): A Three-Layered Virtual Screening Approach. *Mol. Inform.* **2012**, 45, 4828-4837.

(33) Fourches, D.; Muratov, E.; Ding, F.; Dokholyan, N. V.; Tropsha, A. Predicting Binding Affinity of CSAR Ligands Using Both Structure-Based and Ligand-Based Approaches. *J. Chem. Inf. Model.* **2013**, 53, 1915-1922.

(34) Varela, R.; Cleves, A. E.; Spitzer, R.; Jain, A. N. A Structure-Guided Approach for Protein Pocket Modeling and Affinity Prediction. *J. Comput.-Aided. Mol. Des.* **2013**, 27, 917-934.

(35) Huang, T. W.; Zaretzki, J.; Bergeron, C.; Bennett, K. P.; Breneman, C. M. DR-Predictor: Incorporating Flexible Docking with Specialized Electronic Reactivity and Machine Learning Techniques to Predict CYP-Mediated Sites of Metabolism. *J. Chem. Inf. Model.* **2013**, 53, 3352-3366.

(36) Noha, S. M.; Schmidhammer, H.; Spetea, M. Molecular Docking, Molecular Dynamics, and Structure–Activity Relationship Explorations of 14-Oxygenated *N* -Methylmorphinan-6-Ones as Potent μ-Opioid Receptor Agonists. *ACS Chem. Neurosci.* **2017**, *8*, 1327–1337.

(37) Piazzi, L.; Cavalli, A.; Belluti, F.; Bisi, A.; Gobbi, S.; Rizzo, S.; Bartolini, M.; Andrisano, V.; Recanatini, M.; Rampa, A. Extensive SAR and Computational Studies of 3-{4-[(Benzylmethylamino)Methyl] Phenyl}-6,7-Dimethoxy-2H-2-Chromenone Derivatives. *J. Med. Chem.* **2007**, *50*, 4250–4254.

(38) Charles, M. D.; Brookfield, J. L.; Ekwuru, T. C.; Stockley, M.; Dunn, J.; Riddick, M.; Hammonds, T.; Trivier, E.; Greenland, G.; Wong, A. C.; Cheasty, A.; Crighton, D.; Olson, M.F. Discovery, Development, and SAR of Aminothiazoles as LIMK Inhibitors with Cellular Anti-Invasive Properties. *J. Med. Chem.* **2015**, *58*, 8309–8313.

(39) Deng, Y.; Roux, B. Computations of Standard Binding Free Energies with Molecular Dynamics Simulations. *J. Phys. Chem. B* **2009**, *113*, 2234–2246.

(40) Miller, P. S.; Aricescu, A. R. Crystal Structure of a Human GABAA Receptor. *Nature* **2015**, *512*, 270–275.

(41) Šali, A.; Blundell, T. L. Comparative Protein Modelling by Satisfaction of Spatial Restraints. *J. Mol. Biol.* **1993**, *234*, 779–815.

(42) Puthenkalam, R.; Hieckel, M.; Simeone, X.; Suwattanasophon, C.; Feldbauer, R. V.; Ecker, G. F.; Ernst, M. Structural Studies of GABAA Receptor Binding Sites: Which Experimental Structure Tells Us What? *Front. Mol. Neurosci.* **2016**, *9*, 1–20.

(43) Jones, G.; Willett, P.; Glen, R. C.; Leach, A. R.; Taylor, R. Development and Validation of a Genetic Algorithm for Flexible Docking. *J. Mol. Biol.* **1997**, *267*, 727–748.

(44) Halgren, T. A. Merck Molecular Force Field. II. MMFF94 van Der Waals and Electrostatic Parameters for Intermolecular Interactions. *J. Comput. Chem.* **1996**, *17*, 520–552.

(45) Molecular Operating Environment (MOE), 2013.08; ULC, Chemical Computing Group. 1010 Sherbooke St. West, Suite #910, Montreal, QC, Canada, H3A 2R7 2018.

(46) Verdonk, M. L.; Cole, J. C.; Hartshorn, M. J.; Murray, C. W.; Taylor, R. D. Improved Protein-Ligand Docking Using GOLD. *Proteins* **2003**, *52*, 609–623.

(47) MOL_RMSD, Scientific Vector Language (SVL) Source Code Provided by Chemical Computing Group ULC. 1010 Sherbooke St. West, Suite #910, Montreal, QC, Canada, H3A 2R7 2018.

(48) R. Core Team. R.: A Language and Environment for Statistical Computing; R Foundation for Statistical Computing. Vienna, Austria 2015.

(49) de Leeuw, J.; Mair, P. Multidimensional Scaling Using Majorization: SMACOF in R. *J. Stat. Software, Artic.* **2009**, *31*, 1–30.

(50) Jo, S.; Kim, T.; Iyer, V. G.; Im, W. CHARMM-GUI: A Web-Based Graphical User Interface for CHARMM. *J. Comput. Chem.* **2008**, *29*, 1859–1865.

(51) Brooks, B. R.; Brooks, C. L.; Mackerell, A. D.; Nilsson, L.; Petrella, R. J.; Roux, B.; Won, Y.; Archontis, G.; Bartels, C.; Boresch, S.; Caflisch, A.; Caves, L; Cui, Q.; Dinner, A.R.; Feig, M.; Fischer, S.; Gao, J.; Hodoscek, M.; Im, W.; Kuczera, K.; Lazaridis, T.; Ma, J.; Ovchinnikov, V.; Paci, E.; Pastor, R.W.; Post, C.B.; Pu, J.Z.; Schaefer, M.; Tidor, B.; Venable, R.M.; Woodcock, H.L.; Wu, X.; Yang, W.; York, D.M.; Karplus, M. CHARMM: The Biomolecular Simulation Program. *J. Comput. Chem.* **2009**, *30*, 1545–1614.

(52) Eastman, P.; Friedrichs, M. S.; Chodera, J. D.; Radmer, R. J.; Bruns, C. M.; Ku, J. P.; Beauchamp, K. A.; Lane, T. J.; Wang, L. P.; Shukla, D.; Tye, T.; Houston, M.; Stich, T.; Klein, C.;

Shirts, M.R.; Pande, V.S. OpenMM 4: A Reusable, Extensible, Hardware Independent Library for High Performance Molecular Simulation. *J. Chem. Theory Comput.* **2013**, *9*, 461–469.

(53) Lee, J.; Cheng, X.; Swails, J. M.; Yeom, M. S.; Eastman, P. K.; Lemkul, J. A.; Wei, S.; Buckner, J.; Jeong, J. C.; Qi, Y.; Jo, S.; Pande, V.S.; Case, D.A.; Brooks III, C.L.; MacKerell Jr, A.D.; Klauda, J.B.; Im, W. CHARMM-GUI Input Generator for NAMD, GROMACS, AMBER, OpenMM, and CHARMM/OpenMM Simulations Using the CHARMM36 Additive Force Field. *J. Chem. Theory Comput.* **2016**, *12*, 405–413.

(54) Vanommeslaeghe, K.; MacKerell, a. D. Automation of the CHARMM General Force Field (CGenFF) I: Bond Perception and Atom Typing. *J. Chem. Inf. Model.* **2012**, *52*, 3144–3154.

(55) MacKerell, A. D.; Bashford, D.; Bellott, M.; Dunbrack, R. L.; Evanseck, J. D.; Field, M. J.; Fischer, S.; Gao, J.; Guo, H.; Ha, S.; Joseph-McCarthy, D.; Kuchnir, L.; Kuczera, K.; Lau, F.T.; Mattos , C; Michnick, S.; Ngo, T,; Nguyen, D,T,; Prodhom, B.; Reiher, W.E.; Roux, B.; Schlenkrich, M.; Smith, J.C.; Stote, R.; Straub, J.; Watanabe, M.; Wiórkiewicz-Kuczera, J.; Yin, D.; Karplus, M. All-Atom Empirical Potential for Molecular Modeling and Dynamics Studies of Proteins. *J. Phys. Chem. B* **1998**, *102*, 3586.

(56) Essmann, U.; Perera, L.; Berkowitz, M. L.; Darden, T.; Lee, H.; Pedersen, L. G. A Smooth Particle Mesh Ewald Method. *J. Chem. Phys.* **1995**, *103*, 8577–8593.

(57) Michaud-Agrawal, N.; Denning, E. J.; Woolf, T. B.; Beckstein, O. MDAnalysis: A Toolkit for the Analysis of Molecular Dynamics Simulations. *J. Comput. Chem.* **2011**, *32*, 2319–2327.

(58) Liu, K.; Watanabe, E.; Kokubo, H. Exploring the Stability of Ligand Binding Modes to Proteins by Molecular Dynamics Simulations. *J. Comput.-Aided. Mol. Des.* **2017**, *31*, 201–211.

(59) Wolber, G.; Langer, T. LigandScout: 3-D Pharmacophores Derived from Protein-Bound Ligands and Their Use as Virtual Screening Filters. *J. Chem. Inf. Model.* **2005**, *45*, 160–169.

(60) Hunter, J. D. Matplotlib: A 2D Graphics Environment. *Comput. Sci. Eng.* **2007**, *9*, 90–95.

(61) Chodera, J. D.; Mobley, D. L.; Shirts, M. R.; Dixon, R. W.; Branson, K.; Pande, V. S. Alchemical Free Energy Methods for Drug Discovery: Progress and Chanllenges. *Curr. Opin. Struct. Biol.* **2012**, *21*, 150–160.

(62) Hansen, N.; Van Gunsteren, W. F. Practical Aspects of Free-Energy Calculations: A Review. *J. Chem. Theory Comput.* **2014**, *10*, 2632–2647.

(63) Tembe, B. L.; Cammon, J. A. M. Ligand-Receptor Interactions. *Comput. Chem.* **1984**, *8*, 281–283.

(64) Labute, P. The Generalized Born/Volume Integral Implicit Solvent Model: Estimation of the Free Energy of Hydration Using London Dispersion Instead of Atomic Surface Area. *J. Comput. Chem.* **2008**, *29*, 1693–1698.

(65) Corbeil, C. R.; Williams, C. I.; Labute, P. Variability in Docking Success Rates Due to Dataset Preparation. *J. Comput.-Aided Mol. Des*. **2012**, 26, 775–786.

(66) Farid, R.; Day, T.; Friesner, R. A.; Pearlstein, R. A. New Insights about HERG Blockade Obtained from Protein Modeling, Potential Energy Mapping, and Docking Studies. *Bioorganic Med. Chem.* **2006**, *14*, 3160–3173.

(67) Trott, O.; Olson, A. J. Software News and Update AutoDock Vina: Improving the Speed and Accuracy of Docking with a New Scoring Function, Efficient Optimization, and Multithreading. *J. Comput. Chem.* **2010**, *31*, 455–461.

(68) Ebert, V.; Scholze, P.; Sieghart, W. Extensive Heterogeneity of Recombinant γ-Aminobutyric Acid(A) Receptors Expressed in A4β3γ2-Transfected Human Embryonic Kidney 293 Cells. *Neuropharmacology* **1996**, *35*, 1323–1330.

(69) Chen, C.; Okayama, H. High-Efficiency Transformation of Mammalian Cells by Plasmid DNA. *Mol. Cell. Biol.* **1987**, *7*, 2745–2752.

(70) Yung-Chi, C.; Prusoff, W. H. Relationship between the Inhibition Constant (KI) and the Concentration of Inhibitor Which Causes 50 per Cent Inhibition (I50) of an Enzymatic Reaction. *Biochem. Pharmacol.* **1973**, *22*, 3099–3108.

(71) Fryer, R. I.; Zhang, P.; Rios, R.; Gu, Z. Q.; Basile, A. S.; Skolnick, P. Structure-Activity Relationship Studies at the Benzodiazepine Receptor (BZR): A Comparison of the Substituent Effects of Pyrazoloquinolinone Analogs. *J. Med. Chem.* **1993**, 1669–1673.

(72) Simeone, X.; Siebert, D. C. B.; Bampali, K.; Varagic, Z.; Treven, M.; Rehman, S.; Pyszkowski, J.; Holzinger, R.; Steudle, F.; Scholze, P.; Mihovilovic, M.D.; Schnuerch, M.; Ernst, M. Molecular Tools for GABAA Receptors: High Affinity Ligands for B1-Containing Subtypes. *Sci. Rep.* **2017**, *7*, 1–12.

(73) He, X.; Huang, Q.; Yu, S.; Ma, C.; McKernan, R.; Cook, J. M. Studies of Molecular Pharmacophore/Receptor Models for GABAA/BzR Subtypes: Binding Affinities of Symmetrically Substituted Pyrazolo[4,3-c]Quinolin-3-Ones at Recombinant Alpha x Beta 3 Gamma 2 Subtypes and Quantitative Structure-Activity Relationship Studi. *Drug Des. Discov.* **1999**, *16*, 77–91.

(74) Ananthan, S.; Clayton, S. D.; Ealick, S. E.; Wong, G.; Evoniuk, G. E.; Skolnick, P. Synthesis and Structure-Activity Relationships of 3,5-Disubstituted 4,5-Dihydro-6H-Imidazo[1,5-a][1,4]Benzodiazepin-6-Ones at Diazepam-Sensitive and Diazepam-Insensitive Benzodiazepine Receptors. *J. Med. Chem.* **1993**, *36*, 479–490.

(75) Kruskal, J. B. Multidimensional Scaling by Optimizing Goodness of Fit to a Nonmetric Hypothesis. *Psychometrika* **1964**, *29*, 1–27.

(76) Liu, K.; Watanabe, E.; Kokubo, H. Exploring the Stability of Ligand Binding Modes to Proteins by Molecular Dynamics Simulations. *J. Comput.-Aided. Mol. Des.* **2017**, *31*, 201–211.

(77) Friesner, R.A.; Banks J.L.; Murphy, R.B.; Halgren, T.A.; Klicic, J.J.; Mainz, D.T.; Repasky, M.P.; Knoll, E.H.; Shelley, M.; Perry, J.K.; Shaw, D.E.; Francis, P.; Shenkin, P.S. Glide: A New Approach for Rapid, Accurate Docking and Scoring. 1. Method and Assessment of Docking Accuracy. *J. Med. Chem.* **2004**, *47*, 1739–1749.

(78) Gould, R. G.; Jacobs, W. A. The Synthesis of Certain Substituted Quinolines and 5,6-Benzoquinolines. *J. Am. Chem. Soc.* **1939**, *61*, 2890–2895.

(79) Ogris, W.; Pöltl, A.; Hauer, B.; Ernst, M.; Oberto, A.; Wulff, P.; Höger, H.; Wisden, W.; Sieghart, W. Affinity of Various Benzodiazepine Site Ligands in Mice with a Point Mutation in the GABA A Receptor Γ2 Subunit. *Biochem. Pharmacol.* **2004**, *68*, 1621–1629.

(80) Ross, G. A.; Morris, G. M.; Biggin, P. C. One Size Does Not Fit All: The Limits of Structure-Based Models in Drug Discovery. *J. Chem. Theory Comput.* **2013**, 10, 4266-4274

(81) Da, C.; Mooberry, S. L.; Gupton, J. T.; Kellogg, G. E. How to Deal with Low-Resolution Target Structures: Using SAR, Ensemble Docking, Hydropathic Analysis, and 3D-QSAR to Definitively Map the Aβ-Tubulin Colchicine Site. *J. Med. Chem.* **2013**, *56*, 7382–7395.

(82) Sarkar, A.; Kellogg, G. E. Hydrophobicity--Shake Flasks, Protein Folding and Drug Discovery. *Curr. Top. Med. Chem.* **2010**, *10*, 67–83.

(83) Ritchie, T. J.; Macdonald, S. J. F.; Peace, S.; Pickett, S. D.; Luscombe, C. N. The Developability of Heteroaromatic and Heteroaliphatic Rings – Do Some Have a Better Pedigree as Potential Drug Molecules than Others? *MedChemComm* **2012**, 3, 1062.

(84) Savini, L.; Chiasserini, L.; Pellerano, C.; Filippelli, W.; Falcone, G. Synthesis and Pharmacological Activity of 1,2,4-Triazolo[4,3-a]Quinolines. *Farmaco* **2001**.

(85) Bento, A. P.; Gaulton, A.; Hersey, A.; Bellis, L. J.; Chambers, J.; Davies, M.; Krüger, F. A.; Light, Y.; Mak, L.; McGlinchey, S.; Overington, J.P. The ChEMBL Bioactivity Database: An Update. *Nucleic Acids Res.* **2014**, *42*. 1083-90

(86) Peltason, L.; Bajorath, J. SAR Index: Quantifying the Nature of Structure-Activity Relationships. *J. Med. Chem.* **2007**, *50*, 5571–5578.

(87) Vihinen, M.; Torkkila, E.; Riikonen, P. Accuracy of Protein Flexibility Predictions. *Proteins Struct. Funct. Bioinforma.* **1994**, 19, 141-149.

(88) Yaseen, A.; Nijim, M.; Williams, B.; Qian, L.; Li, M.; Wang, J.; Li, Y. FLEXc: Protein Flexibility Prediction Using Context-Based Statistics, Predicted Structural Features, and Sequence Information. *BMC Bioinformatics* **2016**, 17, 281

Table of Contents graphic.